Energy Economics 132 (2024) 107459

Contents lists available at ScienceDirect

Energy Economics

journal homepage: www.elsevier.com/locate/eneeco

Model-driven multimodal LSTM-CNN for unbiased structural forecasting of European Union allowances open-high-low-close price

Wenyang Huang [a], Jianyu Zhao [b], Xiaokang Wang [c,*]

[a] College of Economics and Management, China Agricultural University, 100083 Beijing, China
[b] College of Electronics and Information Engineering, Beihang University, 100191 Beijing, China
[c] School of Economics and Management, Beijing University of Posts and Telecommunications, 100876, Beijing, China

ARTICLE INFO

Keywords:
Multimodal LSTM-CNN
Unbiased structural forecast
OHLC data
EUA
EU ETS

ABSTRACT

European Union allowances (EUAs), the "currency in circulation" of the EU Emissions Trading Scheme (ETS), have spawned a great deal of speculative trading. This study proposes a model-driven long short-term memory network (LSTM)-convolutional neural network (CNN) hybrid model that integrates numerical data features and candlestick features to achieve accurate and unbiased structural prediction of EUA futures open-high-low-close (OHLC) prices during the four phases of the EU ETS. During EU ETS Phase IV, the out-of-sample prediction outcomes of the LSTM-CNN model exhibited a mean absolute percentage error (MAPE) of 0.942%, a mean absolute error (MAE) of 0.877, a root mean squared error (RMSE) of 1.157, a goodness-of-fit (R^2) of 0.953, an accuracy ratio (AR) of 0.544, and a forecast correct rate of ups and downs (UP) of 0.579. In comparison to Naive methods, vector autoregression (VAR) combined with vector error correction model (VECM), multiple linear regression (MLR), partial least squares (PLS), support vector regression (SVR), and standalone LSTM, the LSTM-CNN approach demonstrated a notable enhancement in the average MAPE across the four stages of the EU ETS—specifically, an improvement of 21.66%, 43.15%, 15.73%, 15.72%, 10.45%, and 5.91%, respectively. Drawing from the unbiased structural forecasts of OHLC data, this study proposes fruitful intraday trading strategies that attain substantive investment returns in the realm of EUA futures trading. The multimodal forecasting methodology and intraday trading strategies advanced in this study hold considerable promise within the domain of energy finance.

1. Introduction

Anthropogenic emissions of greenhouse gases exert a profound influence on global climate, with carbon dioxide predominantly implicated (Hammoudeh et al., 2014; Ma et al., 2023). Post the 1992 Framework Convention on Climate Change, nations have striven to stabilize and curtail greenhouse gas (GHG) emissions (Hickmann, 2014). The European Union Emissions Trading System (EU ETS), originating from the 1997 Kyoto Protocol consensus, epitomizes the cornerstone of the EU's endeavors to mitigate climate change (Tan and Wang, 2017). At present, the EU ETS spans nearly 9500 power stations, manufacturing plants, and flights across 30 countries within the European Economic Area, representing approximately 36% of the EU's total GHG emissions (European Commission, 2022). For over a decade, the EU ETS has played a pivotal role in the cost-effective reduction of GHG emissions from the EU's power, industry, and aviation sectors (Wei et al., 2021).

Instituted in 2005, the EU ETS operates as a compulsory "cap and trade" scheme (Bayer and Aklin, 2020). The EU ETS mechanism imposes a cap on aggregate CO_2-equivalent GHG emissions, subsequently lowering emissions over time and ultimately reducing the overall emissions (European Commission, 2023). Annually in February, each regulated entity receives a specified quantity of European Union Allowances (EUAs) (Huang et al., 2022a). Each EUA entitles regulated organizations to emit one ton of CO_2-equivalent GHG (Ellerman et al., 2016). In April of each year, regulated enterprises must surrender sufficient EUAs to offset their GHG emissions from the preceding year (Dhamija et al., 2017). Enterprises that curtail emissions below assigned quotas can trade surplus allowances, whereas those surpassing quotas must procure supplementary allowances or incur substantial penalties (Wang et al., 2022b). The EU ETS engenders incentives for investments in emissions-reducing equipment and, in theory, facilitates the most cost-effective emissions reductions (Viteva et al., 2014).

* Corresponding author.
E-mail addresses: hwy96@cau.edu.cn (W. Huang), jyzhao@buaa.edu.cn (J. Zhao), xiaokang.wang@bupt.edu.cn (X. Wang).

https://doi.org/10.1016/j.eneco.2024.107459
Received 7 December 2023; Received in revised form 18 February 2024; Accepted 27 February 2024
Available online 6 March 2024

The operational mechanisms of the EU ETS render EUA a unique productive asset and, more significantly, a tradable financial commodity (Batten et al., 2020). Numerous studies have observed substantial speculative traders in EUA markets (Chevallier, 2010; Lu and Wang, 2011; Zheng et al., 2015; Rannou et al., 2021). Despite speculative activities inducing volatility in EUA prices, engendering market instability, and potentially culminating in price bubbles (Jeszke and Lizak, 2021), speculators also contribute to the EUA price discovery process and market liquidity (Lucia et al., 2015). Given the financial nature of EUA, the fundamental incentive mechanism to maintain its efficacy is driven by investors' continuous buying and selling to reap profits (Liu et al., 2017; Tan and Wang, 2017). For speculators, precise forecasting of EUA futures prices are crucial for hedging their portfolios and generating returns (Huang et al., 2022a). Furthermore, accurate forecasting of EUA prices offers several merits. Firstly, for over a decade, regulated entities have mitigated their exposure to carbon trading in the spot market by holding EUA futures (Liu et al., 2017). Dependable projections of EUA futures prices are significant for regulated enterprises to manage their portfolios, thereby minimizing production risks (Alberola et al., 2008; Chevallier, 2011). Secondly, discerning future EUA price trends enables policymakers to evaluate the efficacy of the EU ETS and implement necessary modifications (Koch et al., 2014). For instance, the European Commission can promptly adjust the carbon cap by considering the trade-off between EUA prices and low-carbon technology optimization costs for enterprises (Wei et al., 2021). This approach facilitates the establishment of a more efficient and stable carbon market, promoting cost-effective emission reductions (Hintermann et al., 2016). Thirdly, unambiguous signals from EUA price forecasts can incentivize enterprises to invest in low-carbon technologies, thereby contributing to long-term emissions reduction objectives (Creti et al., 2012).

In the EUA trading market, futures trading volume surpasses spot and over-the-counter (OTC) trading, establishing itself as the most important EUA traded commodity (Kossoy and Guigon, 2012; Koch et al., 2014). Existing literature on EUA futures price forecasting can be broadly categorized into three primary stages and types. Early research focused on traditional econometric models, including generalized autoregressive conditional heteroscedastic model (GARCH) (Chevallier and Sévi, 2011), vector error correction models (VECM) (Creti et al., 2012), quantile regression (Tan and Wang, 2017), autoregressive integrated moving average model (ARIMA) (Sheng et al., 2020), multiple linear regression (MLR) (Batten et al., 2020), and partial least squares regression (PLS) (Zhang and Tang, 2023a). The advantages of econometric models encompass model setup simplicity and robust explanatory power; however, they are unable to effectively capture the non-linearity and non-normality of EUA futures prices, resulting in suboptimal prediction accuracy (Qin et al., 2022).

The evolution of computer technology has ushered in a new era in the forecasting of EUA futures prices, with the application of machine learning and artificial neural network models renowned for their significant nonlinear learning capabilities. Notably, models such as radial basis function neural network (RBFNN) (Tsai and Kuo, 2014), multilayer perceptron (MLP) (Fan et al., 2015), the Markov chain Monte Carlo method (Kim et al., 2017), random forest (RF) (Pawłowski, 2021), long short-term memory network (LSTM) (Zhang and Xia, 2022), and least squares support vector machine regression (LSSVM) (Zhu et al., 2022). These models can effectively capture the nonlinear characteristics of EUA futures prices, exhibiting high forecasting accuracy and robustness; nevertheless, they also exhibit drawbacks, such as slow convergence, susceptibility to local optima, and complex parameter optimization (Wang et al., 2022b).

In recent years, EUA futures price forecasting models have advanced towards hybrid models, aiming to achieve more accurate forecasts. Examples include ARIMA and LSSVM (Zhu and Wei, 2013), variation mode decomposition (VMD) and spiking neural networks (SNNs) (Sun et al., 2016), empirical mode decomposition (EMD) and LSSVM (Zhu et al., 2017), time series complex network analysis technology (CPN) and extreme learning machine algorithm (ELM) (Xu et al., 2020), GARCH and LSTM (Huang et al., 2021b), GARCH and gated recurrent unit (GRU) (Yun et al., 2022), CEEMDAN, VMD, permutation entropy (PE), and multiple machine learning models (Nadirgil, 2023), CEEMDAN and LSTM (Yun et al., 2023), VMD, complete ensemble empirical mode decomposition with adaptive noise (CEEMDAN), LSSVM, AND LSTM (Zhang and Tang, 2023b), extremely randomized tree (ET), multivariate variational mode decomposition (MVMD), and LSTM (Zhang et al., 2023a), EMD and ELM (Zhang et al., 2023b), singular spectrum analysis (SSA) and SVR (Zhang et al., 2023c). These models effectively circumvent the limitations of univariate models, offering high prediction accuracy; however, they exhibit complex structures and require extensive computational resources (Li et al., 2021; Wang et al., 2022b).

Despite the utilization of various models (linear or nonlinear), explanatory variables (exogenous or endogenous), and data with diverse frequencies (high or low frequency) to predict EUA futures prices, a notable issue in the majority of the literature is the exclusive focus on EUA futures close prices. In financial markets, EUA futures prices manifest as open-high-low-close (OHLC) data (Huang et al., 2022b). Apart from the close price, intraday trading information encompasses open price, high price, and low price (Huang et al., 2024a). The structural forecasting of OHLC data can enable investors to devise more profitable trading plans than relying solely on close price forecasts. Examples of such benefits include obtaining overnight returns (Cooper et al., 2008), reducing fund holding periods (Dunis et al., 2011), lowering overnight exposure (Kelly and Clark, 2011), and deriving better profits from high-low price range trades (von Mettenheim and Breitner, 2012). A structural forecast method for EUA futures OHLC prices was initially proposed by Huang et al. (2022a). They employed OHLC data for three days preceding the EUA futures price, along with economic, energy, and weather exogenous variables from the previous day, to structurally forecast the EUA futures OHLC price for that day. Out-of-sample modeling demonstrates the remarkable forecast capability of convolutional neural network (CNN) with a mean absolute percentage error (MAPE) of 1.371%, outperforming the Naive method, vector auto-regression (VAR), VECM, MLR, support vector regression (SVR), and MLP. Based on the structural prediction results of the in-sample OHLC data, three novel trading strategies with higher Sharpe ratios compared to the traditional close-to-close strategy are proposed.

Acknowledging that Huang et al. (2022a) achieved structural prediction of EUA futures OHLC data through the proposed unconstrained transformation method, it suffers from two shortcomings. Firstly, Huang et al. (2022a) fail to consider the valuable information embedded in the EUA futures price candlestick charts. Numerous scholars have highlighted the critical role of candlestick chart patterns for price forecasting (Goo et al., 2007; Lu et al., 2012; Tsai and Quan, 2014; Chen et al., 2016; Liang et al., 2022; Cagliero et al., 2023). The feature fusion of both numerical and graphical data will play an essential role in further enhancing model forecast accuracy. Secondly, the OHLC data forecasting process of Huang et al. (2022a) consists of three steps and leads to biased estimates. The first step is to convert the OHLC data of the raw EUA futures prices into unconstrained data through unconstrained transformation. The second step involves time series modeling for the unconstrained data forecasts. The third step is to reduce the obtained unconstrained forecasts back to the original OHLC data. In time series modeling, the loss function set by Huang et al. (2022a) aims to minimize the sum of squares of deviations between the unconstrained forecast results and the original unconstrained data. This does not guarantee minimum error between the obtained OHLC data prediction results and the original OHLC data. Even if the predictions of the transformed variables are unbiased, when reverting to the original variables, it is crucial to consider the underlying expectation transformation. Jensen's inequality points out that biased estimation arises during the expectation transformation of a convex function (Needham, 1993). While Huang et al. (2023a) put forth a model-driven loss function setting for

the structural forecasting of OHLC data in the context of Shanghai crude oil futures, its seamless integration with artificial neural networks (ANNs) remains limited. Furthermore, in comparison to the contributions made by Huang et al. (2023a), this study introduces more intricate intraday trading strategies.

To address these gaps, this study proposes a novel model-driven LSTM-CNN hybrid model, facilitating the fusion of both numerical and candlestick chart features. This integration aims to enable accurate forecasting of EUA futures OHLC prices throughout the distinct phases (Phase I to IV) of the EU ETS. The model-driven loss function is configured to ensure that the loss sum of squares of the interested OHLC forecasts is minimized. Within this hybrid architecture, the LSTM is adopted to extract features from the EUA futures OHLC data, while the CNN is designed to capture features from the candlestick charts. Diverse information from multiple sources of heterogeneous data undergoes an integration process via feature fusion. Subsequently, this consolidated information is systematically channeled into the tail fully connected neural network, ultimately yielding the forecasts of EUA futures OHLC prices. The contributions of this study are threefold: (1) Firstly, it introduces a model-driven method for achieving unbiased forecasts of EUA futures OHLC prices. This enriches the existing structural modeling paradigm for handling complex data. The OHLC structured forecasting results can be instrumental for investors in the EUA market, enabling the formulation of profitable investment strategies and thereby fostering liquidity within the EUA market. (2) Secondly, this study puts forth a feature fusion-based LSTM-CNN framework for EUA futures price forecasting. This innovative framework adeptly integrates both numerical and graphical information. Its adaptability extends beyond EUA futures to encompass other price forecasts within the energy sector, including commodities such as coal, gas, and electricity. (3) Thirdly, this study delves into the long-time modeling window widths across the four phases of the EU ETS. This unique perspective provides historical and forward-looking considerations for the EUA futures price forecasting efforts. The dataset, spanning from April 22, 2005, to November 6, 2023, encompasses a total of 4768 samples.

The structure of the study is organized as follows. Section 2 introduces the development of the EU ETS. Section 3 presents the literature review. Section 4 describes the candlestick chart and OHLC data, as well as research data. Section 5 introduces the employed methods. Section 6 presents the forecast results of the proposed feature fusion LSTM-CNN method. Section 7 provides a summary and brief conclusion of this study.

2. The European Union emission trading scheme

The EU ETS has gone through three phases to date: Phase I (2005–2007), Phase II (2008–2012), and Phase III (2013−2020), making a significant contribution to the reduction of the EU's GHG emissions. Ex-post evidence indicates that the EU ETS saved approximately 1.2 billion tons of CO_2 between 2008 and 2016 (3.8%) compared to a scenario without the EU ETS (Bayer and Aklin, 2020). Abrell et al. (2011) also provided micro-level evidence that the EU ETS impacted enterprises' emission reductions without affecting profit performance by using the panel data from >2000 European enterprises from 2005 to 2008. EUA has become an indispensable production resource and an important financial trading product (Huang et al., 2022a). For more than a decade, regulated enterprises have been able to reduce their exposure to carbon trading in the spot market by holding EUA futures (Liu et al., 2017). Speculators earned profits by buying and selling EUA futures and provided good liquidity for EUAs (Tan and Wang, 2017). The cumulative volume of EUA futures from 4/1/2005 through 12/31/2021 of up to 87.1 billion CO_2-equivalent showcased its vigorous trading dynamics and demonstrated the importance of the EU ETS (European Commission, 2023). As the largest, most liquid, and influential GHG emission reduction mechanism involving emissions worldwide, the EU-ETS offers an effective model for countries around the world to implement emissions trading (Wei et al., 2021).

Table 1 presents the characteristics of the three phases of the EU ETS and their insufficiencies. In general, the development history of the EU ETS's three phases involves four milestones. (1) The allocation mechanism transitioning from a "bottom-up" National Allocation Plan (NAP) to a "top-down" National Implementation Measure (NIM), with the carbon emission cap gradually decreasing (Huang et al., 2022a). (2) The EUA allocation mechanism evolving from free-allocation-based to auction-allocation-based, increasingly reflecting the "polluter pays" principle (Sato et al., 2022). (3) The scope of countries, industries, and

Table 1
Characteristics and insufficient of the first three phases of the EU ETS.

Phase	Characteristic	Insufficient
Phase I (2005–2007)	• Pilot phase to achieve a learning-by-doing experience (Aatola et al., 2013). • Almost all EUAs were allocated for free based on the National Allocation Plan (NAP) (Convery, 2009). • No >5% of EUAs were auctioned (Hepburn et al., 2006). • Covered only CO_2 emissions from the power generators and energy-intensive industries (European Commission, 2023). • Inter-phase banking of EUAs was not allowed (European Commission, 2023).	• Phase I of the EU ETS failed to furnish adequate incentives for GHG mitigation (Lepone et al., 2011). • Towards the end of Phase I, EUAs were in massive surplus, leading to price volatility and structural breakdowns (Skjærseth and Wettestad, 2009). • The convoluted and non-transparent NAP design in each country hindered incentives for low-carbon investments by enterprises (De Perthuis and Trotignon, 2014).
Phase II (2008–2012)	• The transition phase aimed to promote members to meet concrete emissions reduction targets (Creti et al., 2012). • NAP remained predominant, with a cap reduction of 6.5% compared to the 2005 level (European Commission, 2023). • No >10% of EUAs were auctioned (Hepburn et al., 2006). • Nitrous oxide emissions from nitric acid production were included in regulation (European Commission, 2023). • Inter-phase banking of EUAs was allowed (Hintermann et al., 2016).	• New issues such as VAT fraud and cyber-attacks surfaced, which had a negative impact on the reputable image of the EU ETS (Aatola et al., 2013). • Most countries continued to allocate EUAs based on historical emissions, penalizing enterprises that had already reduced carbon emissions and others planning to adopt low-carbon strategies (Sartor et al., 2014). • Allocations to new installations provide high and frequent fuel differentiation subsidies, risking significant distortion in investment decisions (Neuhoff et al., 2006).
Phase III (2013–2020)	• Reform phase to ensure the European target of 20% GHG emission reduction by 2020, relative to 1990 level (Creti et al., 2012). • The National Implementation Measure (NIM) was adopted to replace NAP. Each country's EUAs were uniformly allocated by the European Commission (Dai et al., 2021). • The proportion of auctions was no <30% and reached 70% in 2020 (Mirzaee Ghazani and Jafari, 2021). • The aviation sector was officially included in the EU ETS (Batten et al., 2020). • The "Market Stabilization Reserve" program was approved and implemented, transferring 900 million tons of EUA surpluses to the reserve market from 2014 to 2016 (Huang et al., 2022a).	• An excessive number of sectors were designated as "at risk of leakage" and thus received free allowances, extending issues of potential windfall profits (Laing et al., 2013). • There were serious price bubbles in the EU ETS (Creti and Joets, 2017). The primary cause was the EU ETS's susceptibility to industry changes and policy adjustments in each country due to its extensive industry coverage and broad participation from numerous countries (Wei et al., 2022). • The shipping industry remained at risk of carbon leakage, which is anticipated to be addressed in Phase IV of the EU ETS (Wu et al., 2022).

enterprises covered gradually expanding. (4) Carbon quotas progressively allow inter-term borrowing and storage of quotas, incentivizing enterprises to undertake energy-saving and emission-reduction actions as early as possible and encouraging them to develop long-term emission reduction plans (European Commission, 2023). Although there were insufficient in the first three phases of the EU ETS, it is worth acknowledging that these early practices effectively reduced political resistance to EU carbon reduction, accelerated the process of building a trading market, and provided a lot of lessons for the improvement of subsequent mechanism (Meadows et al., 2019; Flachsland et al., 2020).

Commencing on January 1, 2021, the EU ETS officially entered Phase IV. To achieve the goal of a 40% reduction in greenhouse gas (GHG) emissions compared to 1990 levels, the European Commission has implemented several significant reforms to the EU ETS. These reforms include four main aspects. (1) Acceleration of decreasing total allowances. The overall number of emission allowances declines at an annual rate of 2.2% from 2021 onwards, compared to 1.74% in Phase III. (2) Significant changes to the MSR. The MSR is designed to stabilize allowance prices by reducing the quantity in circulation (i.e., the supply of allowances minus the demand) and to increase the resilience of the EU ETS to future shocks. The initial provision was that if the total number of allowances in circulation exceeded 833 million, 12% of the allowances would be transferred to the MSR. As part of the Phase IV revisions, this has been increased to 24% per year for 2019 to 2023. Starting in 2023, allowances in the MSR that exceed a specific threshold will be annulled. (3) Reform of the coverage industries. In July 2021, the European Commission proposed reforms to include intra-EU maritime emissions in the ETS and to create separate ETSs for buildings and road transport emissions. (4) Revised carbon leakage rules. Sectors facing the highest risk of carbon leakage will continue to receive 100% of the free allocation (at baseline levels, which are also being recalculated), while those considered less at risk will be phased out of the free allocation after 2026. In Phase IV, the baseline value determining the level of free allocation for each installation will be updated twice to prevent windfall profits and reflect technological advances since 2008 (Perino, 2018).

These ambitious reforms hold the potential to ensure the smooth operation of Phase IV of the EU ETS and provide abundant opportunities and a broad market for EUA futures trading (Hu et al., 2015). The MSR will reduce the number of tradable EUAs, maintaining them at a competitively priced level (Bruninx et al., 2020). The reduced likelihood of a structural break in EUA prices will attract more regulated enterprises and speculators to trade EUAs. Although the total quota amount in Phase IV is decreasing more rapidly than in previous phases, the increasing percentage of auctions will render EUA futures a more essential strategic production reserve and a more active financial trading product. In the context of the EU ETS entering a new phase and the global economic rebound, reliable forecasting of EUA futures prices in EU ETS Phase IV is crucial for investors and regulated enterprises to manage and hedge their portfolios for profit and risk reduction (Huang et al., 2022a), as well as providing important reference indicators for government macro-control and policy formulation (Wang et al., 2022b). In addition to tracking the EUA price forecasts for Phase IV of the EU ETS, it is equally interesting to realize the EUA price forecasts for the first three phases of the EU ETS, which facilitates the testing of the predictive accuracy and robustness of the proposed forecasting model.

Fig. 1 displays the OHLC prices for EUA from April 22, 2005 to November 6, 2023, with each day of data represented as a candlestick chart. Specifically, (1) in Phase I of the EU ETS, due to the lack of historical data and allocation experience, the total amount of free allocation of EUA grossly exceeded the actual emissions, which led to a significant drop in EUA futures from a high of 37.697 USD/ton on April 19, 2006 to 8.413 USD/ton on December 14, 2006. Since the EUA from Phase I could not be stored for Phase II, in the second half of 2007, the EUA futures price approached zero (Hintermann, 2010); (2) In Phase II of the EU ETS, the global financial crisis in the second half of 2008 and the European debt crisis in the second half of 2011 led to a surplus of commodities and a decline in production capacity, which in turn led to a decrease in the demand side of the EUA and a sharp decline in the EUA futures price (Huang et al., 2022a); (3) In Phase III of the EU ETS, the "Market Stabilization Reserve" (MSR) program diverted 900 million tons of EU quota surpluses from 2014 to 2016 to the reserve market, significantly reducing the supply of EUA. A large number of speculators entered the market, causing the price of EUA to rise from 5.195 USD/ton on April 3, 2017 all the way to 33.241 USD/ton on July 23, 2019. The outbreak of COVID-19 in late 2019 led to a significant reduction in EUA demand, lowering EUA prices to March 23, 2020 at 16.660 USD/ton. The EUA futures price increased again between April 2020 and December 2020 as COVID-19 was contained and socio-economic recovery took place, eventually closing at the end of Phase III at 39.118 USD/ton (Huang et al., 2022a); (4) During Phase IV of the EU ETS, EUA prices showed a rapid upward trend in general, and most especially in 2021. In 2021, EUA futures prices surged from 41.264 USD/ton at the beginning of the year to 91.683 USD/ton at the end of the year, an increase of 122.186%. This phenomenon is the result of the mismatch between supply and demand. On the one hand, the total amount of EUA quota is decreasing on the supply side. On the other hand, the European energy crisis, the sharp rise in natural gas prices, and extreme weather led to an increase in the use of high-carbon emission coal, which greatly increased the demand for EUA. In 2022, EUA futures market activity declined due to the wave of geopolitical risks, investor confidence was low, and EUA futures fluctuated violently around the price pivot of 85 USD/ton. On February 24, 2022, the Russian-Ukrainian conflict erupted

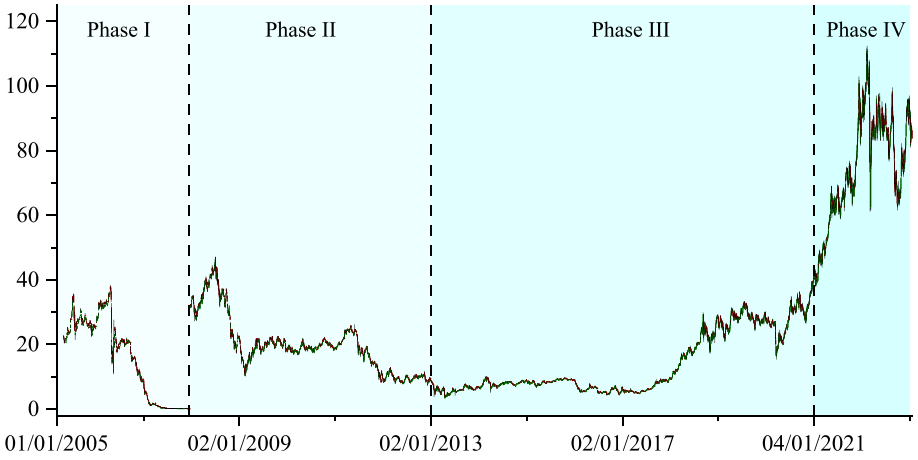

Fig. 1. Candlestick charts of EUA futures prices from April 22, 2005 to November 6, 2023 (Unite: USD/ton). Data source: DataStream.

and EUA futures prices plummeted 9.41% in a single day (Zhang et al., 2024). With the de-escalation of the Russia-Ukraine conflict situation and the unchanged ambitions of climate policy, market investment confidence has been revitalized, which has been very supportive of EUA prices. The Nord Stream gas pipeline explosion on September 26, 2022, triggered a substantial surge in European gas prices. In response, some industrial companies found themselves compelled to resort to highly polluting coal for their energy supply, leading to a notable uptick in the demand for EUA. From late 2022 to the first half of 2023, the EUA futures price center lifted to near 95 USD/ton and reached a historical high point of 105.522 USD/ton on April 11, 2023. As the latter half of 2023 unfolded, the EU grappled with a looming energy crisis, accentuated by ongoing geopolitical conflicts, particularly in the Middle East. Consequently, EUA futures prices have sustained their elevated position, holding steady at 90 USD/ton.

3. Literature review

Forecasting the price of EUA futures has garnered substantial interest in both academia and industry, which is crucial for market speculators in devising profitable investment strategies (Tan and Wang, 2017), regulated companies in hedging production risks (Chevallier, 2011), policymakers in evaluating the effectiveness of the EU ETS (Koch et al., 2014), and companies in incentivizing investment in low-carbon technologies (Creti et al., 2012).

Some early studies employed univariate or multivariate linear models, including VECM (Creti et al., 2012), MLR (Guðbrandsdóttir and Haraldsson, 2011), ARIMA and VARMA (vector ARMA) (García-Martos et al., 2013). The agglomerative nature and spiky, thick-tailed features of carbon price fluctuations have spurred the application of GARCH-type models for EUA futures price forecasting. For instance, Paolella and Taschini (2008), Chevallier and Sévi (2011), Lutz et al. (2013), and Byun and Cho (2013) have verified the exceptional forecasting performance of various GARCH-type models during Phase I and II of the EU ETS. However, these econometric models exhibit two key disadvantages: (1) their implementation primarily relies on linear assumptions and stationary data, rendering them inadequate for capturing the nonlinear characteristics of carbon prices (Qin et al., 2022), and (2) their applicability is limited to forecasting small-sample datasets (Zhang et al., 2022). These drawbacks significantly hinder their predictive performance and the applicability of statistical models (Zhang et al., 2023b).

With advancements in big data and computer technology, the highly nonlinear characteristics of EUA futures prices have gained considerable attention in the realm of carbon price forecasting (Li et al., 2016). Consequently, machine learning methods have been extensively employed to capture the nonlinear characteristics of EUA futures prices and achieve accurate predictions (Huang et al., 2022a). Univariate examples include Tsai and Kuo (2014) implemented real-time prediction of EUA futures prices using RBFNN; Fan et al. (2015) developed a MLP for EUA futures prices forecast based on phase reconstruction; García and Jaramillo-Morán (2020) also utilized MLP to achieve short-term forecasts of EUA futures prices and obtained an average error of 1.7617%; Pawłowski (2021) employed a RF model to predict the subsequent day's EUA futures price, with results demonstrating that the proposed model outperformed the classical linear model; Zhu et al. (2022) proposed a novel multi-objective LSSVM with a hybrid kernel to achieve accurate prediction of EUA spot and futures prices. Zhang and Wen (2022) proposed a novel deep neural network model called TCN-Seq2Seq to predict EUA futures prices from April 22, 2005 to December 29, 2017. The model employs a "sequence-to-sequence" layout and uses only fully convolutional layers to learn temporal data dependencies, resulting in a significant reduction in training parameters. It was found that TCN-Seq2Seq outperformed ARIMA, RF, XGBoost, SVR, and LSTM in terms of predictive ability and robustness.

In recent years, forecasting EUA futures prices utilizing hybrid models has witnessed significant advancements. Among these, the most notable is the decomposition-ensemble forecasting methodology, which initially deconstructs the original carbon price series through various techniques, predicts sub-series utilizing distinct models, and ultimately merges them to generate the predicted values for the original series (Huang et al., 2021b). For instance, Sun et al. (2016) developed a combined prediction model incorporating VMD and spiking neural networks (SNNs). Initially, VMD decomposed the original carbon futures price series into a set of relatively stable components. A SNN prediction model was then constructed for each component, and the aggregation of predictions for all components produced the final prediction of the raw carbon futures price. The study demonstrated that the proposed VMD-SNN prediction model outperformed traditional models regarding prediction accuracy and reliability. Liu and Shen (2020) employed the empirical wavelet transform (EWT) to decompose carbon futures price data into trend, low-frequency, and high-frequency components. Subsequently, the GRU neural network predicted each component's values, which were aggregated to form the final combined prediction of the original carbon price. The results indicated that the prediction accuracy of the EWT-GRU surpassed that of ARIMA, back propagation neural network (BPNN), and GRU. (Huang et al., 2021b) proposed a novel decomposition-ensemble paradigm, the VMD-GARCH/LSTM-LSTM model. After employing VMD to divide the carbon futures price series into sub-models, the LSTM predicted the low-frequency sub-mode while the GARCH model predicted the high-frequency sub-mode. The results revealed that the proposed model exhibited exceptional performance in carbon futures price prediction. Li et al. (2023) combined the multiple ensemble patch transform (MEPT) and improved complete ensemble empirical mode decomposition with adaptive noise (ICEEMDAN) to efficiently capture multi-resolution trends and volatility patterns of EUA futures prices. They also employed a causal temporal convolutional network (CTCN) to simultaneously achieve accurate forecasting of EUA prices and appropriate causal inference. The empirical results showed that the proposed MEPT-ICEEMDAN-CTCN model obtained satisfactory MAPE in multi-step forecasting.

Additional hybrid research includes Zhu and Wei (2013) developed a hybrid model integrating ARIMA and LSSVM to predict four carbon futures prices. Furthermore, particle swarm optimization (PSO) was utilized to identify the optimal LSSVM parameters to enhance prediction accuracy. Empirical results highlighted the appeal of the proposed hybrid approach for carbon price forecasting. Xu et al. (2020) proposed a new carbon futures price prediction model based on CPN and ELM. Empirical analysis indicated that the CPN-ELM model can improve the ELM's prediction accuracy in terms of both horizontal and directional accuracy while exhibiting greater robustness in the face of random samples, data with different frequencies, and data with structural changes. Yun et al. (2022) constructed a novel hybrid model called NAGARCHSK-GRU. The GARCH-type model extracted time-varying, high-order moment parameter features of carbon futures prices, and the multi-layer GRU model was trained with the obtained time-varying parameters. Results revealed that the proposed model had good accuracy and robustness for carbon price forecasting. In addition, the long-term prediction performance was also validated.

Upon reviewing prior studies, we identified the following potential research gaps in carbon price forecasting. (1) The majority of existing literature concentrated solely on EUA futures' close price forecasts, rather than structural forecasts of EUA futures' OHLC price data. The close-to-close trading strategy fails to provide investors with detailed decision support and forfeits a considerable amount of potential profit (Cooper et al., 2008; Kelly and Clark, 2011; von Mettenheim and Breitner, 2012). (2) Huang et al. (2022a) achieved the first structural prediction of OHLC prices for EUA futures. However, two shortcomings persist. Firstly, their EUA futures price forecasting relies exclusively on numerical variables, neglecting the wealth of information encapsulated within graphical candlestick charts. In fact, studies by Kim and Kim (2019), Shin et al. (2019), Chen and Tsai (2020), and Hung et al. (2020,2021) have demonstrated the superior predictive power of

candlestick charts for financial products. Secondly, according to Jensen's inequality, the expectation transformation process between unconstrained results and OHLC results leads to biased forecasting outcomes. It cannot be ensured that the obtained OHLC prediction results have the minimum mean square error, which may lead to a decrease in prediction accuracy (Huang et al., 2023a). (3) Most forecasting studies have focused on EU ETS Phases I to III, with very few predictions of EUA prices in Phase IV. However, changes in carbon market mechanisms (e.g., accelerating decline in total emission caps, MSR rule revisions, and increase in EUA auction proportion) and the complexity of the global economy (e.g., the demand recovery after the COVID-19 outbreak) may result in highly volatile carbon prices in Phase IV (Wei et al., 2023). This raises the ongoing concern about whether the highly volatile carbon prices in Phase IV can be accurately forecasted.

To address these gaps, this study proposes a novel model-driven LSTM-CNN forecast framework for the OHLC prices of the EUA in Phase IV of the EU ETS. The framework aims to provide a more comprehensive and accurate prediction by incorporating the rich information contained in candlestick charts and addressing the issues related to the expectation transformation process. By focusing on the challenges posed by Phase IV, this study aims to contribute to the ongoing efforts in carbon price forecasting and provide valuable insights for investors and policymakers alike. In addition, the first three phases of the EU ETS are modeled in this study using the proposed model to test its predictive performance and robustness.

4. Data description

4.1. Candlestick chart and pattern recognition

Candlestick charts originated in the rice market during the Tokugawa Shogunate era (1603–1867) in Japan. According to legend, a Japanese trader named Munehisa Homma carefully observed the changes in the price of rice in the market every day and marked the fluctuations in the price of rice with a graph to analyze and predict the market price of rice and the pattern of ups and downs, which is the prototype of candlestick charts (Varadharajan and Vikkraman, 2011). Later, Steve Nison introduced the theory of candlestick charting, which was a great success in the East, to the West in the 1990s, and gradually developed to maturity (Nison, 1994).

The advantages that candlestick analysis has over other technical analysis methods are that (1) candlestick charts have precise definitions and they respond to good market signals; and (2) with the rise of behavioral finance, scholars have found that investor sentiment is an important determinant of financial market behavior (Caginalp and Laurent, 1998). By tracking daily price movements, candlestick charts reveal the forces of demand and supply within the financial markets, reflecting the overall mood and movement of investors. Candlestick charting has become the most intuitive and widely used method of analyzing market price movements. It is not limited by language, and investors can judge from the shape of the candles the long and short transactions during the trading time, and roughly judge the future trend (Tsai and Quan, 2014).

Candlestick charts reflect the first traded price (open price), the highest traded price (high price), the lowest traded price (low price), and the last traded price (close price) over a period of time (Huang et al., 2022b). This time frame can range from a few seconds to several months. In technical analysis, the most common time range is days. Fig. 2 gives an illustration of a daily candlestick chart of EUA futures. The EUA futures market lasts from 8:00 a.m. until 6:00 p.m. Central European Time (CET), with no breaks in between. A candlestick chart consists of a real body, an upper shadow, and a lower shadow, visualizing the size of the difference between any two prices. Candlestick charts can be bullish or bearish, with green indicating a bullish market where the close price is greater than the open price, while red indicates a bearish market where the open price is greater than the close price. The technical analysis method developed based on candlestick charts is known as pattern recognition. Scholars working on pattern recognition try to find certain recurring shapes in candlestick charts to predict future changes in prices, and thus to time their buys and sells to make profits (Santur, 2022; Chen et al., 2023). Some common bull and bear rollover candlestick patterns include three white soldiers, three black crows, morning star, and evening star (Nison, 1994; Chen and Tsai, 2020).

4.2. OHLC data and numerical analysis

The OHLC data is a numerical vector representation of candlestick charts. There is a one-to-one correspondence between candlestick charts and OHLC data. From the perspective of symbolic data analysis, OHLC data belongs to a special form of interval data: OHLC data uses the high and low prices as the upper and lower boundaries of the interval, and compared to traditional interval data, it also includes the open and close prices inside the interval, which is an expansion of interval data. According to Huang et al. (2023b), the mathematical definition of OHLC data is shown below.

Definition 1. A four-dimensional vector $x_t = \left(x_t^{(o)}, x_t^{(h)}, x_t^{(l)}, x_t^{(c)}\right)'$ is considered typical OHLC data if it satisfies the following three constraints:

1. Positive constraint: $x_t^{(l)} > 0$;
2. Interval constraint: $x_t^{(l)} < x_t^{(h)}$;
3. Boundary constraint: $x_t^{(o)}, x_t^{(c)} \in \left[x_t^{(l)}, x_t^{(h)}\right]$.

Here $x_t^{(o)}$ is the t period daily open price, $x_t^{(h)}$ is the t period daily high price, $x_t^{(l)}$ is the t period daily low price, and $x_t^{(c)}$ is the t period daily close price.

The technical analysis method developed based on OHLC data is called numerical analysis. Numerical analysis is based on the idea that historical information affects future movements, and focuses on

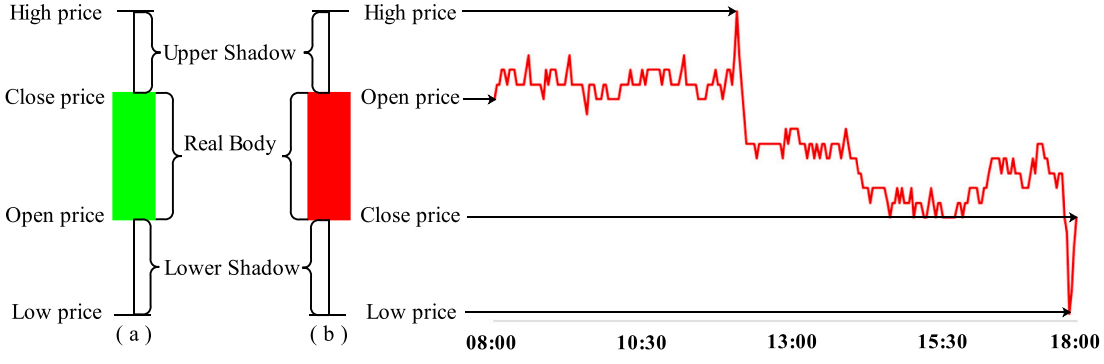

Fig. 2. An illustration of EUA futures candlestick chart (a) Bullish (b) Bearish.

portraying trends, cycles, and non-stationary behavior in the four-dimensional time series of OHLC data, with the results often presented in numerical form (Gu et al., 2023; Wang, 2022; Wang et al., 2022a; 2023). Numerical analysis gives a more direct prediction of prices, allowing investors to plan their purchases and sales according to price movements, and to realize the goal of buying low and selling high (Huang et al., 2023a).

For structural prediction of OHLC data, the focus is to always ensure that the prediction results satisfy the constraint formulas within the OHLC data. Otherwise, investors will not be able to make effective decisions based on the forecast results and strike investment confidence. That is to say, for the OHLC series $TS = \{\mathrm{x}_t\}_{t=1}^{T}$, its forecast result of $(T+m)$ $(m \in R^{+})$ period must be ensured that: (1) $\widehat{x}_{T+m}^{(l)} > 0$; (2) $\widehat{x}_{T+m}^{(l)} < \widehat{x}_{T+m}^{(h)}$; and (3) $\widehat{x}_{T+m}^{(o)}, \widehat{x}_{T+m}^{(c)} \in \left[\widehat{x}_{T+m}^{(l)}, \widehat{x}_{T+m}^{(h)}\right]$ (Huang et al., 2024b). Obviously, these constraints are not guaranteed to be valid if we apply the time series prediction method directly to the original OHLC data. The structural forecasting methods for OHLC data are discussed in Section 5.1.

4.3. Data selection

This study collects daily EUA futures OHLC data traded on the Intercontinental Exchange (ICE) and related technical indicators for EU ETS Phase I (2005–2007), Phase II (2008–2012), Phase III (2013–2020), and Phase IV (2021−2023). The specific EUA price data selected are shown in Table 2. The expiry date of the EUA futures under consideration is December 21. The reasons for choosing this particular EUA futures are threefold. Firstly, in the year 2010, ICE completed the acquisition of the European Climate Exchange (ECX), seamlessly integrating its carbon trading operations into ICE's European futures business. Notably, ECX stands out as the largest carbon trading platform within the EU ETS, and it typically accounts for >80% of the daily carbon trading volume in the EU's key carbon markets (Gong et al., 2023). Secondly, EUA futures exhibit more stable price structures (Chevallier, 2009), higher trading volumes (Kossoy and Guigon, 2012), and better price discovery than EUA spot prices (Reboredo, 2013). Thirdly, December 21st EUA futures represent the most actively traded EUA futures product (Huang et al., 2022a). The data for this variable is sourced from the DataStream database (https://www.refinitiv.com/en). For instances where data is missing, we employ interpolated values from preceding and subsequent periods as supplements.

For the graphical candlestick chart corresponding to the OHLC data, we have the following settings. In general, at least three candlestick charts are needed to identify patterns (Nison, 2001). For example, the morning star pattern and evening star pattern (Lv and Hao, 2017), and three line strikes and three black crows (Hung and Chen, 2021). Therefore, in this study, the input to the CNN is a 3-day candlestick charts series and the input to the LSTM is 3-day EUA futures OHLC data and the corresponding technical indicators. Referring to Hung et al. (2020, 2021), the 3-day candlestick charts series employed in this study is a squared, grey-scaled, black backgrounded image of 64 pixels in length and width. The white-colored real body represents a bull market, and the grey real body implies a bear market.

Table 2
Selected EUA futures OHLC data at different phases of the EU ETS.

EU ETS Phases	Time window	Sample size
Phase I	2005/4/22–2007/12/17	681
Phase II	2007/12/19–2012/12/31	1294
Phase III	2013/1/2–2020/12/31	2057
Phase IV	2021/1/4–2023/11/6	736

5. Research methods

5.1. Structural forecasting methods for OHLC data

The inherent constraints of OHLC data initiate challenges to its structural predictive modeling, with the biggest hurdle being how to ensure that the predictive results always follow these constraint equations. The traditional processing method in the field of complex data is to first use the unconstrained transformation to change the OHLC data into unconstrained variables, and then after the prediction of the unconstrained variables, the prediction of the original OHLC data is obtained by the inverse transformation. This practice has been widely used in data types such as interval data (Zhao et al., 2022), compositional data (Wang et al., 2021a), OHLC data (Huang et al., 2022a, 2022b), and functional data (Huang et al., 2021a). Nevertheless, according to Jensen's inequality, the modeling process based on the unconstrained transformation and inverse transformation formulas produces biased estimates during the mean transformation process. In this study, we take the lead in realizing unbiased structural prediction of OHLC prices by designing a model-driven deep learning model loss function.

5.1.1. Traditional unconstrained transformation method

The basic idea of the traditional unconstrained transformation method is to find a mapping transformation $f(\cdot)$ that maps the OHLC data to a four-dimensional full vector space. The unconstrained data obtained after the mapping of the OHLC data by $f(\cdot)$ has to have a clear economic meaning and a one-to-one correspondence with the original OHLC data. And $f(\cdot)$ needs to have an explicit inverse transformation expression $f^{-1}(\cdot)$ The one-to-one correspondence between the original OHLC data $\mathrm{x}_t = \left(x_t^{(o)}, x_t^{(h)}, x_t^{(l)}, x_t^{(c)}\right)'$ and the transformed unconstraint vector $\mathrm{y}_t = \left(y_t^{(1)}, y_t^{(2)}, y_t^{(3)}, y_t^{(4)}\right)'$ can be summarized as Eq. (1) and Eq. (2).

$$\mathrm{y}_t = f(\mathrm{x}_t) = \begin{pmatrix} ln x_t^{(l)} \\ ln\left(x_t^{(h)} - x_t^{(l)}\right) \\ ln\left(\dfrac{\lambda_t^{(o)}}{1-\lambda_t^{(o)}}\right) \\ ln\left(\dfrac{\lambda_t^{(c)}}{1-\lambda_t^{(c)}}\right) \end{pmatrix}. \tag{1}$$

$$\mathrm{x}_t = f^{-1}(\mathrm{y}_t) = \begin{pmatrix} \dfrac{exp\left\{y_t^{(2)} + y_t^{(3)}\right\}}{exp\left\{y_t^{(3)}\right\}+1} + exp\left\{y_t^{(1)}\right\} \\ exp\left\{y_t^{(1)}\right\} + exp\left\{y_t^{(2)}\right\} \\ exp\left\{y_t^{(1)}\right\} \\ \dfrac{exp\left\{y_t^{(2)} + y_t^{(4)}\right\}}{exp\left\{y_t^{(4)}\right\}+1} + exp\left\{y_t^{(1)}\right\} \end{pmatrix}. \tag{2}$$

The $\lambda_t^{(o)}$ and $\lambda_t^{(c)}$ are two proxy data formulated as Eq. (3) and Eq. (4).

$$\lambda_t^{(o)} = \frac{x_t^{(o)} - x_t^{(l)}}{x_t^{(h)} - x_t^{(l)}}, \tag{3}$$

$$\lambda_t^{(c)} = \frac{x_t^{(c)} - x_t^{(l)}}{x_t^{(h)} - x_t^{(l)}}. \tag{4}$$

The value range of each component in Eq. (1) spans from $-\infty$ to ∞, offering the flexibility of the well-known log- and logit- transformations. Furthermore, each component in y_t carries explicit economic significance: (1) $y_t^{(1)}$ reflects the absolute level of EUA futures prices; (2) $y_t^{(2)}$

signifies the intraday trading range, serving as a measure of volatility; (3) $y_t^{(3)}$ and $y_t^{(4)}$ reflect the relative positions of the open and close prices within the boundaries of low-high prices, respectively. In essence, the magnitude of intraday trends and price fluctuations can be fully reflected by y_t, which are assumed to be informative about future price developments.

Based on the proposed unconstrained transformation method, the process of forecasting the OHLC series $TS = \{x_t\}_{t=1}^{T}$ can be realized through a trilogy. Firstly, conduct transformation on each x_t and derive the unconstrained series $UTS = \{y_t\}_{t=1}^{T}$. Secondly, employ a variety of forecasting models to $\{y_t\}_{t=1}^{T}$ and yields the forecaster of $y_{T+m}(m \in \mathbb{R}^+)$, remarked as $\hat{y}_{T+m} = \left(\hat{y}_{T+m}^{(1)}, \hat{y}_{T+m}^{(2)}, \hat{y}_{T+m}^{(3)}, \hat{y}_{T+m}^{(4)}\right)'$. Thirdly, by utilizing the inverse transformation expressed in Eq. (2), we can obtain the corresponding forecaster of x_{T+m} (remarked as $\hat{x}_{T+m} = \left(\hat{x}_{T+m}^{(o)}, \hat{x}_{T+m}^{(h)}, \hat{x}_{T+m}^{(l)}, \hat{x}_{T+m}^{(c)}\right)'$).

The above-mentioned unconstrained transformation Eq. (1), as well as its inverse transformation Eq. (2), provide a novel paradigm for forecasting the OHLC data. The forecast process will guarantee the forecast results adhere to the three inherent constraints listed in Definition 1, thereby actualizing the structural forecasting of the OHLC data. Given the simplicity of the unconstrained transformation method as well as its inverse transformation in the practical application of predictive models, this study applies it to VAR, VECM, MLR, PLS, and SVM modeling.

5.1.2. A novel model-driven loss function setting

The artificial neural network prediction loss function based on the traditional unconstrained transformation method is set as shown in Eq. (5). It is to ensure that the obtained unconstrained vector has the minimum mean square error with its true value. After obtaining the predicted values of the solution constraint vectors, the predicted values of the original OHLC data are then obtained by the inverse transformation equation. According to Jensen's inequality, what is obtained based on the unconstrained transformation and its inverse transformation formula is a biased estimation of the OHLC data, which does not ensure that the predicted OHLC data has the minimum mean square error concerning its true value.

$$\begin{aligned} \mathrm{LOSS} = \sum_{\Omega} \Bigg[& \left(\hat{y}_{T+m}^{(1)} - y_{T+m}^{(1)}\right)^2 + \left(\hat{y}_{T+m}^{(2)} - y_{T+m}^{(2)}\right)^2 \\ & + \left(\hat{y}_{T+m}^{(3)} - y_{T+m}^{(3)}\right)^2 + \left(\hat{y}_{T+m}^{(4)} - y_{T+m}^{(4)}\right)^2 \Bigg]. \end{aligned} \tag{5}$$

In order to avoid the estimation bias caused by the unconstrained transformation method during the mean transformation process, this study proposes a model-driven loss function setting for neural networks. Model-driven loss function setting combines the loss function of the neural network with the inverse transformation formula, which is calculated as follows:

$$\begin{aligned} Model-drivenLOSS = & \sum_{\Omega} \left[\left(\frac{exp\left\{\hat{y}_{T+m}^{(2)} + \hat{y}_{T+m}^{(3)}\right\}}{exp\left\{\hat{y}_{T+m}^{(3)}\right\} + 1} + exp\left\{\hat{y}_{T+m}^{(1)}\right\} \right) - x_{T+m}^{(o)} \right]^2 \\ & + \sum_{\Omega} \left[\left(exp\left\{\hat{y}_{T+m}^{(1)}\right\} + exp\left\{\hat{y}_{T+m}^{(2)}\right\} \right) - x_{T+m}^{(h)} \right]^2 \\ & + \sum_{\Omega} \left[exp\left\{\hat{y}_{T+m}^{(1)}\right\} - x_{T+m}^{(l)} \right]^2 \\ & + \sum_{\Omega} \left[\left(\frac{exp\left\{\hat{y}_{T+m}^{(2)} + \hat{y}_{T+m}^{(4)}\right\}}{exp\left\{\hat{y}_{T+m}^{(4)}\right\} + 1} + exp\left\{\hat{y}_{T+m}^{(1)}\right\} \right) - x_{T+m}^{(c)} \right]^2 \end{aligned} \tag{6}$$

The model-driven loss function setting has two benefits: (1) it can utilize the unconstrained transformation to effectively extract artificial features from the original OHLC data; (2) it can effectively guide the direction of gradient descent of the neural network without increasing the model complexity to ensure that unbiased prediction of the OHLC data structure is obtained. In this study, the model-driven loss function setting is combined with a tail output network of hybrid LSTM and CNN models to ensure that unbiased structural predictions of OHLC data are obtained.

5.2. Neural networks

Traditionally, carbon price prediction has been a challenging endeavor due to the inherent complexity and volatility of carbon markets. While several conventional models, such as ARIMA and GARCH, have made contributions to the prediction landscape, they often struggle with high volatility and nonlinearity inherent in carbon price series. Emerging from this backdrop is a growing interest in the application of artificial intelligence, specifically deep learning models like CNN and LSTM, to predict carbon prices (Ji et al., 2019). CNN and LSTM are able to learn complex patterns from image-based and numeric sequential data, respectively, making them an ideal candidate for predicting carbon futures prices. However, each of them has its unique strengths and limitations, which motivated the development of a hybrid model that leverages the strengths of both architectures.

5.2.1. Convolutional neural network

Convolutional neural networks (CNNs), primarily employed in image processing tasks, have found their way into the time series prediction domain due to their ability to capture local and global dependencies in data (Hoseinzade and Haratizadeh, 2019). They are adept at extracting local features through convolutional layers and identifying patterns within these features, which can then be used for prediction. In the context of carbon futures price prediction, CNN can detect local price patterns and changes in trends, providing valuable insights (Lu et al., 2021). Nonetheless, CNN's performance can be hindered due to its limited capability to recognize long-term dependencies, a crucial aspect of financial time series data. Inspired by the studies of Kim and Kim (2019) and Jiang et al. (2023), this study utilizes CNN to extract features of EUA futures price candlestick charts.

The CNN architecture employed in this study mainly consists of convolutional layers, pooling layers, and a fully connected neural network in the tail. The schematic diagram of CNN is given in Fig. 3.

The convolutional layer extracts different features of the image input through filters as well as convolution operations. In order to fully learn the different features of the image input, several different filters can be used at the same time. As the convolutional layer deepens, the CNN is able to iteratively extract complex features from low-level features such as edges and lines. Define the input to the l-th layer of the CNN as $Z^{(l)} \in \mathbb{R}^{R^{(l)} \times C^{(l)}}$, where $R^{(l)}$ and $C^{(l)}$ are the number of rows and columns of $Z^{(l)}$, respectively. The operational expression for the l-th layer of the CNN is given by

$$Z^{(l+1)} = \mathrm{PL}\left[\Phi\left(W^{(l)} \otimes Z^{(l)}\right) + b^{(l)}\right], \tag{7}$$

where $W^{(l)}$ and $b^{(l)}$ denote the convolution kernel and bias of the l-th layer, respectively, $\Phi(\cdot)$ is the activation function, $\mathrm{PL}(\cdot)$ is the pooling function, and $\otimes$ represents the convolution operation, whose detailed operational expression is:

$$\left[W^{(l)} \otimes Z^{(l)}\right]_{(i,j)} = \sum_{p=1}^{K} \sum_{q=1}^{K} Z^{(l)}{}_{(S(i-1)+p, S(j-1)+q)} W^{(l)}{}_{(p,q)}, \tag{8}$$

where $\left[W^{(l)} \otimes Z^{(l)}\right]_{(i,j)}$ denotes the element in the i-th row and j-th column of the result of the convolutional operation of $W^{(l)}$ and $Z^{(l)}$, $Z^{(l)}{}_{(i,j)}$ represents the element in the i-th row and j-th column of $Z^{(l)}$, K is the

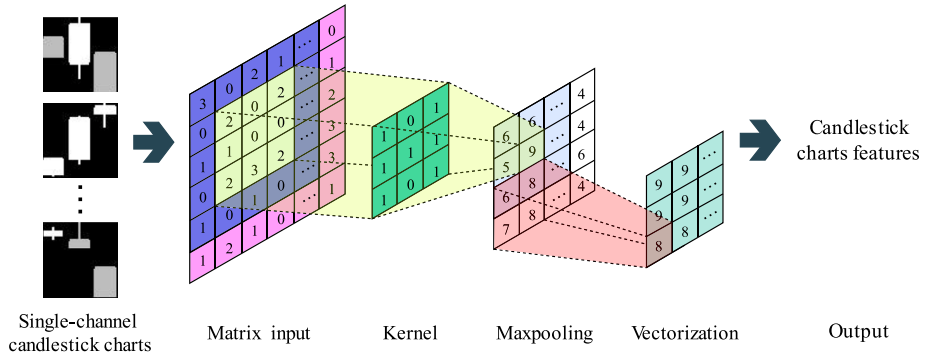

Fig. 3. A typical architecture of CNN.

convolution kernel size (i.e., $W^{(l)} \in \mathbb{R}^{K\times K}$), and S is the convolution kernel step size. For an input matrix, the dimensionality changes after further convolution with a particular filter are:

$$R^{(l+1)} = \frac{R^{(l)} - K + 2p}{S} + 1, \tag{9}$$

$$C^{(l+1)} = \frac{C^{(l)} - K + 2p}{S} + 1, \tag{10}$$

where p denotes the number of boundary pixel layers added to the image edges. p equals to the number of boundary layers added to the image if the boundary pixel padding is in the Same mode, and $p = 0$ if it is in the Valid mode.

The role of the pooling layer in a convolutional neural network is feature fusion and dimensionality reduction. The pooling layer reduces the spatial size of the data by downsampling, so the number of parameters and the amount of computation decreases. Maxpooling is chosen for this study, which is the process of dividing the input image into rectangular regions and outputting the maximum value for each subregion. The dimensionality changes of the input matrix after Maxpooling are:

$$R^{(l+1)} = \frac{R^{(l)} - K}{S} + 1, \tag{11}$$

$$C^{(l+1)} = \frac{C^{(l)} - K}{S} + 1. \tag{12}$$

After several layers of convolution and pooling operations, the obtained features are sequentially expanded by rows, connected into vectors, and input into a fully connected network. The final EUA futures candlestick charts feature information is thus obtained.

5.2.2. *Long short-term memory network*

LSTM well solves the problem of long-term dependence of time series by introducing memory cells and three gating mechanisms and avoids the problem of gradient vanishing or explosion in traditional RNN models (Yu et al., 2019). The memory unit is responsible for storing sequence information, while the three gating mechanisms (forget gate, input gate, and output gate) control the degree of reading, writing, and retention of the memory unit, thus allowing the model to selectively ignore or important information (Graves and Schmidhuber, 2005). In the LSTM model, each time step has an input and an output, the inputs being the current input data and the hidden state of the previous time step, and the outputs being the output of the current time step and the hidden state of the current time step (Sherstinsky, 2020). The parameters of the model are shared over all time steps, so LSTM can handle input sequences of arbitrary length. The disadvantages of LSTMs are that their model structure is relatively complex, training is more time-consuming than CNNs, and they do not parallelize the data very well.

At the current moment t, assuming that the input of the network model consists of two parts: the input x_t at the current moment and the output value h_{t-1} of the hidden layer at the previous moment, and the output state value of the hidden layer at the current moment is calculated and recorded as h_t. The formula of the above process can be expressed as follows:

$$h_t = f(x_t, h_{t-1}) = \sigma(W_{xh}x_t + W_{hh}h_{t-1} + b_h), \tag{13}$$

where W_{xh} is the weight from the input layer to the hidden layer, W_{hh} is the weight from the hidden layer to the hidden layer, b_h is the bias vector of the hidden layer, and σ is the sigmoid function.

Compared to RNN, LSTM introduces a memory unit structure in the hidden layer, which includes three gate controllers: an input gate, a forget gate, and an output gate, which allows the network to forget when to forget historical information and when to update the memory state by applying new information. The structure of the LSTM neurons is schematically shown in Fig. 4.

As illustrated by Fig. 4, all three gates are nonlinear summing units and use multiplication operations and activation functions to control the output. The computation of the LSTM to update the state is divided into the following steps:

(1) Calculate the value of the input gate i_t. The current data information is selectively stored in the memory cell through the input gate, thus affecting the current memory cell state value. The formula of i_t is as follows:

$$i_t = \sigma(W_{xi}x_t + W_{hi}h_{t-1} + b_i), \tag{14}$$

where W_{xi} and b_i are weight parameters and intercept terms of the first part of the input gate to be optimized, respectively.

(2) Calculate temporary memory state information $\widetilde{c}_t$. Before updating the memory unit c_t, a temporary memory is generated unit $\widetilde{c}_t$. And $\widetilde{c}_t$ is jointly generated from the input of the current moment t and the output of the hidden unit of the previous moment $(t-1)$, which are linearly combined with their respective weight matrices to obtain the candidate memory cell value at the current moment and update the memory cell state information.

$$\widetilde{c}_t = tanh(W_{xc}x_t + W_{hc}h_{t-1} + b_c), \tag{15}$$

where W_{xc} and b_c are weight parameters and intercept terms of the second part of the input gate to be optimized, respectively, and tanh is the hyperbolic tangent activation function.

(3) Calculate the value of the forget gate f_t. The forget gate mainly deals with what information in the memory unit needs to be discarded, which is calculated as:

$$f_t = \sigma\left(W_{xf}x_t + W_{hf}h_{t-1} + b_f\right), \tag{16}$$

where W_{xf} and b_f are weight parameters and intercept terms of the forget gate to be optimized, respectively.

(4) Calculate the current moment memory cell state value c_t:

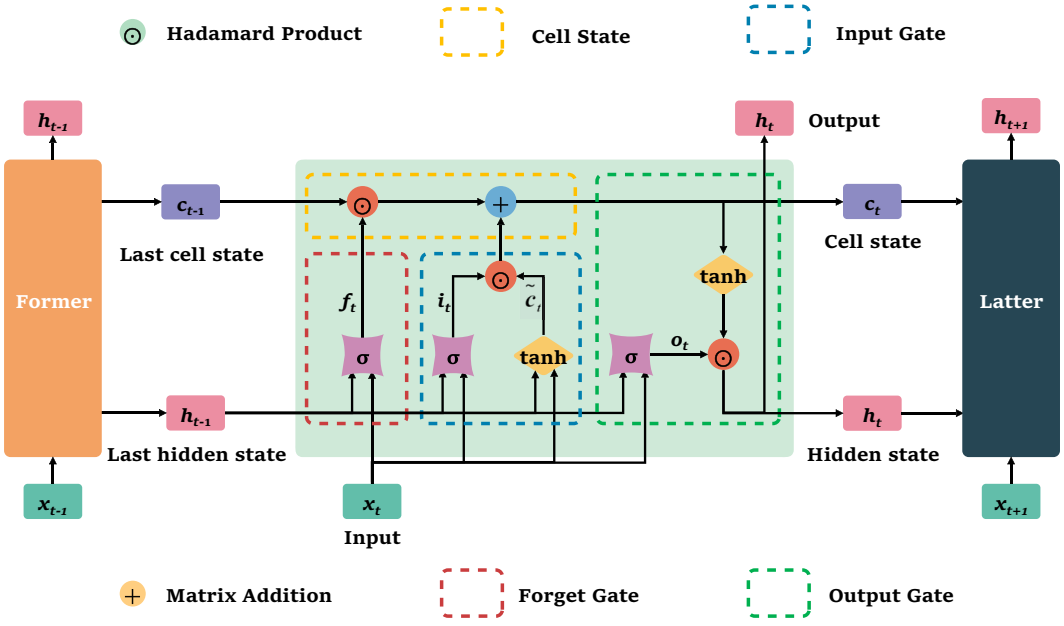

Fig. 4. A typical architecture of the LSTM network.

$$c_t = f_t \odot c_{t-1} + i_t \odot \tilde{c}_t, \tag{17}$$

where $\odot$ is the Hadamard product.

(5) Calculate the output gate o_t. The output gate acts mainly on the output of the state values of the memory cell, whose calculation formula is as follows:

$$o_t = \sigma(W_{xo} x_t + W_{ho} h_{t-1} + b_o), \tag{18}$$

where W_{xo} and b_o are weight parameters and intercept terms of the output gate to be optimized, respectively.

(6) Finally, the output of the LSTM unitary memory h_t is computed as:

$$h_t = o_t \odot tanh(c_t). \tag{19}$$

5.2.3. A hybrid approach: LSTM-CNN

Most of the financial price prediction studies based on hybrid CNN and LSTM models still involve only numerical data (Wu et al., 2021; Wang et al., 2021b; Rostamian and O'Hara, 2022). Although some LSTM-CNN-based studies have considered feature information from both candlestick graphs and historical price numerical data for stock price prediction, the output target is still only the close price (Hoseinzade and Haratizadeh, 2019; Ji et al., 2019; Kim and Kim, 2019).

Given these limitations, this study introduces a hybrid model of CNN and LSTM to leverage the strengths of both models. The hybrid model LSTM-CNN utilizes CNN for feature extraction on candlestick charts of EUA futures prices, while LSTM captures long-term dependencies in historical EUA futures price time series. This combination incorporates comprehensive feature information from multiple sources of heterogeneous data to accurately predict the complex and volatile EUA carbon futures prices. For the graphical and sequential features extracted by CNN and LSTM respectively, they are first concatenated together to form a fused feature vector. The fused features are then fed into a L-layer fully connected neural network (FNN) to obtain structured predictions of OHLC prices through model-driven loss function setting. The computational expression for the above process is as follows:

$$O = \sigma_F\left(W_F^{(L)}\sigma_F\left(\cdots\sigma_F\left(W_F^{(1)}\mathrm{vec}(\widetilde{P},\widetilde{Q}) + b_F^{(1)}\right) + \cdots\right) + b_F^{(L)}\right), \tag{20}$$

where $\mathrm{vec}(\cdot)$ denotes a vectorized operation, $\widetilde{P}$ and $\widetilde{Q}$ represent the graphical features extracted by CNN and the time series features extracted by LSTM, respectively, $W_F^{(l)}$ and $b_F^{(l)}$ are the weights and bias of the l-th layer of the FNN, respectively, and σ_F is the activation function of the FNN. Fig. 5 illustrates a typical hybrid LSTM-CNN modeling process employed in this study.

5.3. Forecast accuracy evaluation indicator

A spectrum of indicators is employed to scrutinize the prediction outcomes of the preceding models. The specific computational formulas for these indicators are delineated below.

(1) The mean absolute percentage error (MAPE) is utilized to measure the average of the absolute percentage errors of forecasts:

$$\mathrm{MAPE} = \frac{1}{4n}\sum_{t=1}^{n}\sum_{*}\frac{\left|\hat{x}_t^* - x_t^*\right|}{\left|x_t^*\right|} \times 100\%, \tag{21}$$

where $\hat{x}_t \in \mathbb{R}^4$ represents the predicted OHLC formed EUA prices on period t; $x_t \in \mathbb{R}^4$ denotes the actual value of OHLC formed EUA prices; * symbolizes the open, high, low, and close prices; and n is the number of forecast periods.

(2) The mean absolute error (MAE) is used to record the mean absolute errors of forecasts:

$$\mathrm{MAE} = \frac{1}{4n}\sum_{t=1}^{n}\sum_{*}\left|\hat{x}_t^* - x_t^*\right|. \tag{22}$$

(3) The root mean squared error (RMSE) is the root mean squared error, reflecting the extent to which forecasted data deviate from actual values:

$$\mathrm{RMSE} = \sqrt{\frac{1}{4n}\sum_{t=1}^{n}\sum_{*}\left|\hat{x}_t^* - x_t^*\right|^2}. \tag{23}$$

(4) The accuracy ratio (AR), as conceptualized by Hu and He (2007), is designed to evaluate the coincidence degree between the forecasted interval and the actual interval:

$$\mathrm{AR} = \frac{1}{n}\sum_{t=1}^{n}\frac{L(\hat{I}_t \cap I_t)}{L(\hat{I}_t \cup I)}, \tag{24}$$

where $I_t = \left[x_t^{(l)}, x_t^{(h)}\right]$ and $\hat{I}_t = \left[\hat{x}_t^{(l)}, \hat{x}_t^{(h)}\right]$; and $L(\cdot)$ is the operator of

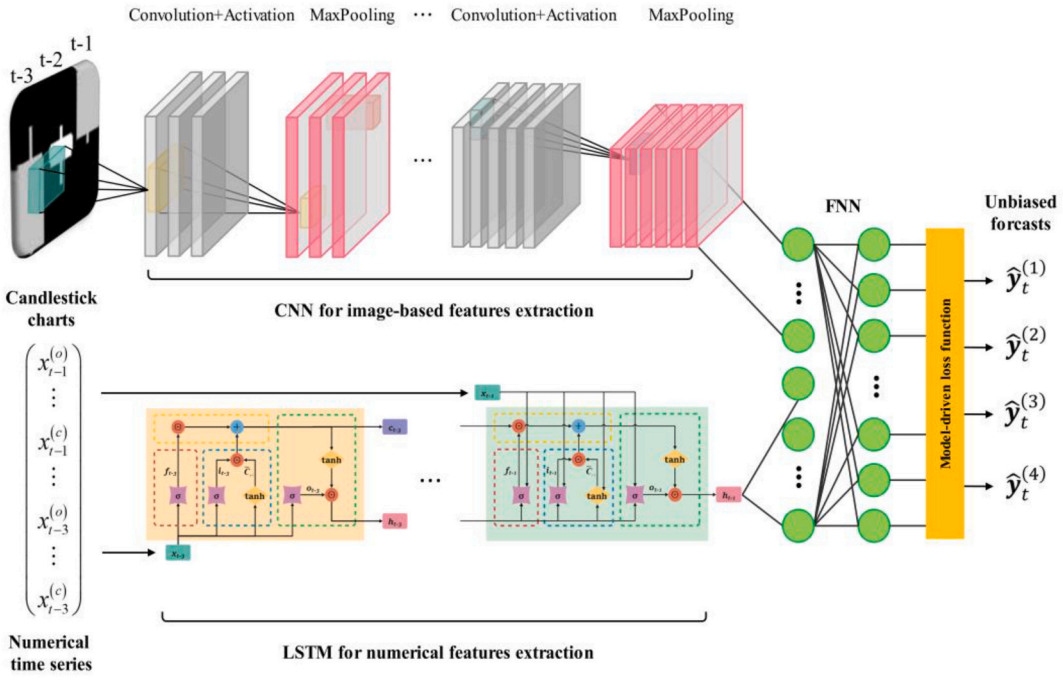

Fig. 5. A hybrid architecture of the LSTM-CNN network.

calculating the length of the interval.

(5) The goodness-of-fit (R^2) measures the overall fit condition of the forecasting model. It is equal to the ratio of the fitted sum of squares to the total sum of squares, i.e., the percentage of EUA futures price variability explained by the forecasting model:

$$R^2 = 1 - \frac{1}{4}\sum^{*} \frac{\sum_{t=1}^{n}\left(\hat{x}_t^{*} - x_t^{*}\right)^2}{\sum_{t=1}^{n}\left(x_t^{*} - \bar{x}_t^{*}\right)^2}, \tag{25}$$

where $\bar{x}_t$ represents the sample mean of a certain time series.

(6) The forecast correct rate of ups and downs (UD) is engineered to assess the model's ability to forecast market trends:

$$UD = \frac{1}{n}\Omega\left(t \middle| \left(\hat{x}_t^{c} - \hat{x}_t^{o}\right)\left(x_t^{c} - x_t^{o}\right) > 0\right), \tag{26}$$

where $\Omega(\cdot)$ is the operator of calculating the number of elements contained in the set.

6. Empirical results

6.1. Model settings

In this study, a variety of prediction models were used in order to comprehensively compare their out-of-sample prediction abilities. Each model was evaluated for accuracy with the chronological top 80% as the training set and the bottom 20% as the test set. The employed models can be categorized into traditional statistical and econometric models, and machine learning models.

Specifically, for traditional statistical and econometric models: (1) the Naive method is an inert algorithm without additional prediction operations, which directly takes the OHLC data of the current day as the predicted value of the next day. In this study, the Naive method serves as a comparative benchmark for the predictive accuracy of other models. (2) VAR and VECM can effectively capture the dynamic cointegration between multivariate time series and are suitable for forecasting modeling of OHLC data. The VAR and VECM in this study use a base modeling window width of 20, i.e., the historical data of the previous 20 sample periods are used on a rolling basis to forecast the next period of OHLC data. (3) MLR is the most basic linear model for multivariate statistical analysis, which generally uses the OLS method for parameter estimation. (4) PLS combines principal component analysis, typical correlation analysis, and multiple linear regression analysis, which can effectively deal with multiple dependent variables and multicollinearity problems. In particular, when the number of principal components extracted by PLS is the same as the number of original variables, the prediction results are the same as those of MLR.

In terms of the machine learning models, there are: (1) SVR stands as a machine learning algorithm grounded in statistical learning theory, showcasing commendable generalization power and short- and medium-term prediction ability. The kernel functions for SVR in this study are chosen to be linear, polynomial, radial, and sigmoid. (2) LSTM takes numerical OHLC historical price data as model input. (3) LSTM-CNN is a hybrid ANN method based on feature fusion and multimodal data, which extracts numerical OHLC price features and candlestick features simultaneously. The hyper-parameter settings for the adoption of LSTM and CNN include a learning rate of 0.00005, batch size of 256, and number of ephemeral elements of 15,000. The LSTM has three layers and the number of hidden nodes in each layer is 160. The CNN has three layers and the number of convolutional kernels in each layer is 6, 24, and 40, the size of the convolutional kernel is 6×6 and maximum pooling is used. The outputs of the LSTM are spliced with the outputs of the CNN and then spliced together after going through the three layers of a FNN to get the output, the numbers of hidden nodes in the three layers of FNN are 300, 300 and 4 respectively. All the activation functions in LSTM, CNN, and FNN are ReLU. The best out-of-sample predictions for each model at various parameter settings and specified number of iterations are reported.

The process of tuning the above hyperparameters involves adjusting the value of one hyperparameter at a time, testing multiple values for each parameter, and identifying the optimal value that yields the best performance among the various tests. After iterating through each hyperparameter, a set of hyperparameters that delivers the best performance can be obtained. In case of the VAR + VECM, MLR, PLS, and SVM, their prediction accuracies are assessed both with and without the application of unconstrained transformation. As for LSTM and LSTM-CNN, their prediction accuracies are evaluated under conditions

involving unconstrained transformation and model-driven loss function settings, as well as without the imposition of unconstrained transformation condition.

6.2. Out-of-sample forecasting results of EU ETS Phase IV

Table 3 gives the metrics for evaluating the accuracy of EU ETS Phase IV EUA futures price forecasts by each model using the unconstrained transformation, and its corresponding graphical presentation is shown in Fig. 6. Fig. 7 further illustrates the raw candlestick charts of EU ETS Phase IV EUA futures prices and the predicted close prices by each model. Table 4, Fig. 8, and Fig. 9 then correspond to the prediction results and accuracy evaluations of the models modeled directly using the raw OHLC data without using the unconstrained transformation. Following a comprehensive analysis, the ensuing conclusions come to the fore:

(1) Leveraging both the unconstrained transformation and the model-driven loss function settings, ANNs exhibit precise forecasting capabilities for EUA futures OHLC prices in Phase IV of the EU ETS. Notably, the hybrid LSTM-CNN model emerges as the best performer in terms of predictive prowess. In the realm of out-of-sample prediction, LSTM-CNN showcased remarkable performance metrics, boasting a 0.942% MAPE, 0.877 MAE, 1.157 RMSE, 0.953 R^2, 0.544 AR, and 0.579 UP. In comparison to the inert Naive algorithm, LSTM-CNN's MAPE, MAE, and RMSE were reduced by 28.690%, 77.120%, and 24.968%, respectively. Additionally, R^2, AR, and UP witnessed increments of 3.587%, 22.523%, and 9.867%, respectively. LSTM, while closely trailing behind, demonstrated commendable figures, including a 1.015% MAPE, 0.946 MAE, 1.227 RMSE, 0.946 R^2, 0.516 AR, and 0.500 UP. These results validate the advantageous impact of incorporating image-based data in enhancing the predictive accuracy of EUA futures prices, affirming the success of the multimodal prediction approach grounded in both numerical and image-based data.

(2) ANNs exhibit heightened predictive accuracy when utilizing the unconstrained transformation, whereas VAR + VECM, MLR, PLS, and SVM perform better without using the unconstrained transformation. When the model inputs take the form of unconstrained vectors, the performance metrics for ANNs, encompassing LSTM and LSTM-CNN, exhibit notable improvements. The average MAPE stands at 0.979%, MAE at 0.912, RMSE at 1.192, R^2 at 0.950, AR at 0.530, and UP at 0.540. These metrics collectively surpass the performance of ANNs utilizing the original OHLC data directly as inputs. The unconstrained transformation, in this context, can be perceived as an artificial feature extraction process. It evidently proves beneficial in enhancing the prediction accuracy of ANNs. Conversely, the VAR + VECM, MLR, PLS, and SVM employed without the unconstrained transformation yield an average MAPE of 1.034%, MAE of 0.960, RMSE of 1.254, R^2 of 0.947, AR of 0.506, and UP of 0.457. Remarkably, these metrics outperform the prediction results under the unconstrained transformation condition, suggesting that these models are more adept at capturing information directly from the original OHLC prices.

(3) Prediction models without using the unconstrained transformation method may encounter prediction failures. For the structural prediction of OHLC data, it is important to ensure that the forecasted results $\widehat{\boldsymbol{x}}_{T+m} = \left(\widehat{x}^{(o)}_{T+m}, \widehat{x}^{(h)}_{T+m}, \widehat{x}^{(l)}_{T+m}, \widehat{x}^{(c)}_{T+m}\right)'$ adhere to the following three constraints: (1) $\widehat{x}^{(l)}_{T+m} > 0$; (2) $\widehat{x}^{(l)}_{T+m} < \widehat{x}^{(h)}_{T+m}$; and (3) $\widehat{x}^{(o)}_{T+m}$, $\widehat{x}^{(c)}_{T+m} \in \left[\widehat{x}^{(l)}_{T+m}, \widehat{x}^{(h)}_{T+m}\right]$. When modeling directly with raw OHLC data, VAR + VECM, MLR, PLS, and SVR exhibit 23, 11, 1, and 2 instances of forecast failures in EU ETS Phase IV EUA futures price forecasts, respectively. These forecast failures typically occur when the predicted open and close prices breakthrough the boundaries set by the low and high prices, i.e., $\widehat{x}^{(o)}_{T+m}, \widehat{x}^{(c)}_{T+m} \notin \left[\widehat{x}^{(l)}_{T+m}, \widehat{x}^{(h)}_{T+m}\right]$. The Naive method, where the current day's OHLC data is used directly as the next day's prediction value, avoids prediction errors but lacks accuracy. On the other hand, LSTM and LSTM-CNN, characterized by high prediction accuracy, do not incur prediction errors. In contrast, the modeling approach based on the unconstrained transformation ensures a structured prediction of OHLC data, thereby guaranteeing consistency in investors' decision-making processes and bolstering their confidence in investment decisions. Furthermore, VAR + VECM without the unconstrained transformation method appears inadequately modeled, predicting only 75 values out of 146 periods. This is clearly illustrated by the discontinuous predicted close price point values in Fig. 9. The phenomenon is attributed to the non-stationary and non-significant cointegration relationship inherent in the original OHLC data quadratic time series.

Table 3
Forecasting accuracy of EUA price in EU ETS Phase IV for each model using unconstrained transformation.

Models	MAPE	MAE	RMSE	R^2	AR	UP
Naive	1.321%	3.833	1.542	0.920	0.444	0.527
VAR + VECM	1.282%	1.195	1.529	0.939	0.435	0.425
MLR	1.112%	1.038	1.326	0.937	0.493	0.308
PLS	1.112%	1.038	1.326	0.937	0.493	0.308
SVR	1.042%	0.965	1.256	0.944	0.508	0.322
LSTM	1.015%	0.946	1.227	0.946	0.516	0.500
LSTM-CNN	0.942%	0.877	1.157	0.953	0.544	0.579
Non-ANNs Average	1.137%	1.059	1.359	0.939	0.482	0.341
ANNs Average	0.979%	0.912	1.192	0.950	0.530	0.540

6.3. Out-of-sample forecasting results of EU ETS Phase I to III

In this study, an extension of the proposed modeling approach involves predicting EUA futures prices for the first three phases of the EU ETS, with the MAPE results presented in Table 5. Notably, the proposed LSTM-CNN hybrid model exhibits optimal MAPE outcomes across all four phases of the EU ETS. Specifically, for Phase I, Phase II, Phase III, and Phase IV of the EU ETS, the LSTM-CNN, utilizing the unconstrained transformation and model-driven loss function, yields MAPE values of 11.035%, 1.089%, 1.499%, and 0.942%, respectively. Compared with Naive method, VAR + VECM, MLR, PLS, SVR, and LSTM, the average MAPE of LSTM-CNN at each stage of the EU ETS is improved by 21.66%, 43.15%, 15.73%, 15.72%, 10.45%, and 5.91%, respectively. These results underscore the commendable prediction accuracy and robustness exhibited by the proposed LSTM-CNN method in forecasting EUA futures prices. Furthermore, concerning the prediction outcomes for EU ETS Phase III EUA futures prices, the MAPE achieved by the proposed LSTM-CNN in this study stands at 1.499%. This signifies a notable optimization of 9.426% when contrasted with the out-of-sample MAPE of 1.655% obtained by Huang et al. (2022a) utilizing a 1-D CNN.

In evaluating the forecasting accuracy of the LSTM-CNN in EU ETS Phase IV, this study extends the analysis by comparing the performance of the proposed model-driven loss function setting with the penalty term-based loss function setting introduced by Huang et al. (2023a). The MAPE results for the penalty term-based loss function setting are detailed in Table 6. It is observed that when the penalty term coefficient is relatively small (e.g., 100 or 200) and the penalty term is incorporated into the loss function from the initial epoch, prediction failures ensue. Conversely, when the penalty term coefficient is relatively large (e.g., 500 or 1000), although the prediction accuracy diminishes, prediction failures are averted. Notably, incorporating a penalty term into the loss function after a certain number of iterations indeed enhances prediction accuracy, aligning with the findings of Huang et al. (2023a). In contrast, LSTM-CNN achieves a MAPE of 0.942% with the loss function setting based on the penalty term (refer to Table 3), surpassing the overall MAPE obtained with the penalty term-based loss function setting. This underscores the superior performance of the proposed model-driven approach in enhancing prediction accuracy compared to the penalty term-based approach.

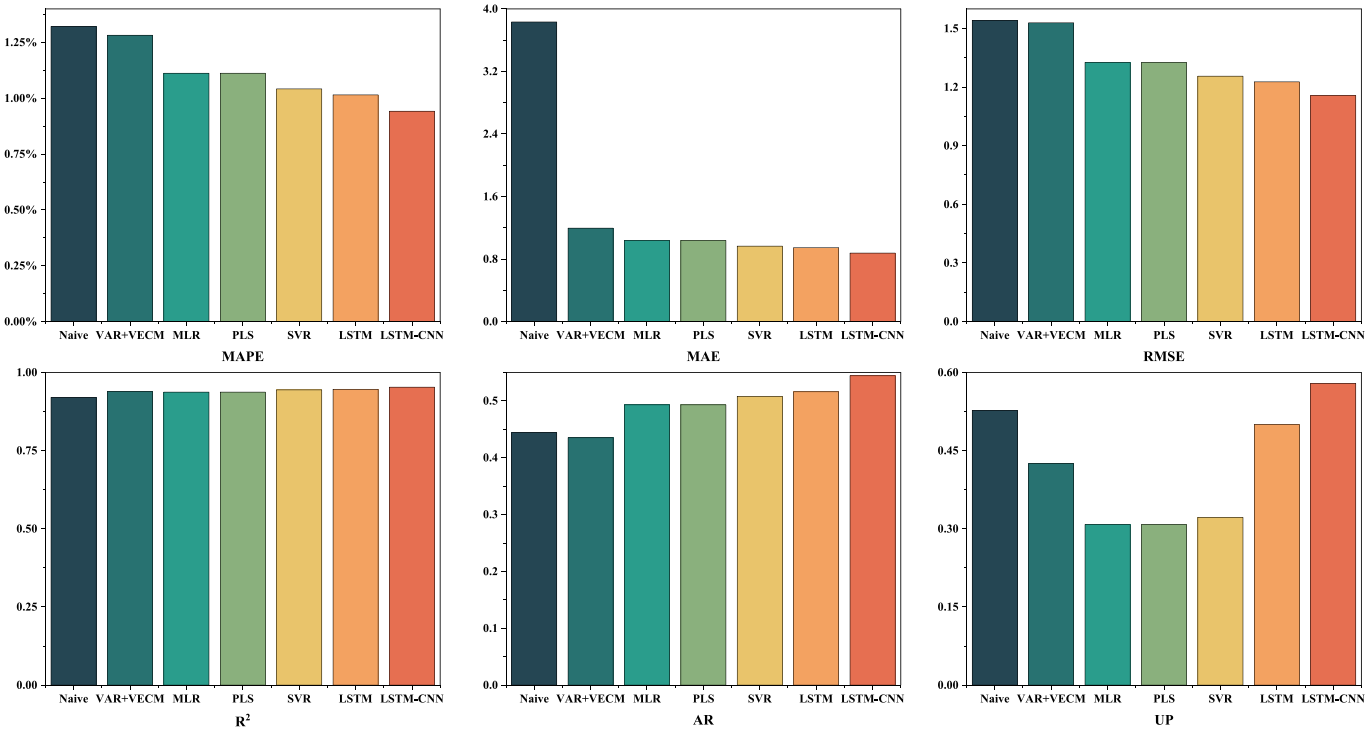

Fig. 6. Forecasting accuracy metrics for each model using unconstrained transformation during EU ETS Phase IV.

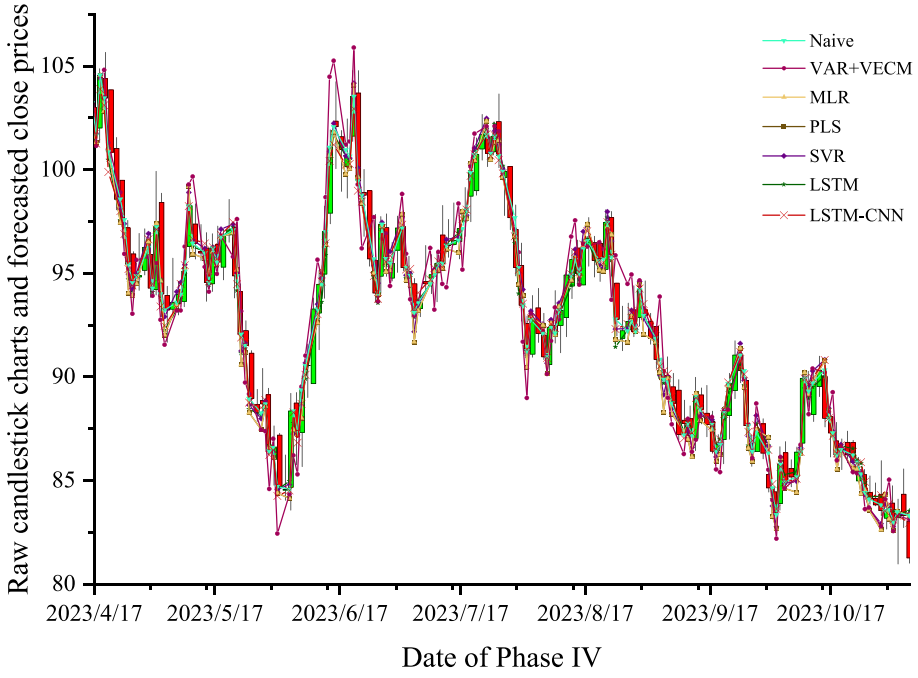

Fig. 7. Raw candlestick charts for EUA futures in EU ETS Phase IV and predicted close prices for each model using unconstrained transformation.

6.4. *Intraday trading strategies leveraging OHLC data*

Utilizing the predicted OHLC data, this study formulates corresponding intraday trading strategies with the objective of executing low buy and high sell transactions to generate trading profits. The trigger conditions, along with designated buying price, selling price, and holding period for each trading strategy are summarized in Table 7. The subscript t signifies the last timestamp of the actual OHLC data observation for EUA futures that is available, and $(t+1)$ denotes the subsequent day to be predicted.

The prevailing literature on EUA futures price forecasting has primarily concentrated on close price prediction, giving rise to corresponding trading strategies such as the close-to-close (long) strategy and close-to-close (short) strategy. The close-to-close (long) strategy entails adopting a long trading position when a rise is predicted for the following day, i.e., $\widehat{x}_{t+1}^{(c)} > \widehat{x}_{t}^{(c)}$. It involves buying at $x_{t}^{(c)}$ to open the position and selling at $x_{t+1}^{(c)}$ to close it, with a holding period of 24:00 h.

Table 4
Forecasting accuracy of EUA price in EU ETS Phase IV for each model without using unconstrained transformation.

Models	MAPE	MAE	RMSE	R^2	AR	UP	Failure
Naive	1.321%	3.833	1.542	0.920	0.444	0.527	0
VAR + VECM	1.209%	1.111	1.433	0.939	0.422	0.412	23
MLR	0.997%	0.930	1.217	0.948	0.529	0.418	11
PLS	0.961%	0.897	1.174	0.951	0.537	0.527	1
SVR	0.967%	0.902	1.192	0.950	0.534	0.469	2
LSTM	1.022%	0.954	1.242	0.945	0.534	0.514	0
LSTM-CNN	0.956%	0.891	1.169	0.952	0.549	0.514	0
Non-ANNs Average	1.034%	0.960	1.254	0.947	0.506	0.457	9.25
ANNs Average	0.989%	0.923	1.206	0.949	0.542	0.514	0

In contrast, the close-to-close (short) strategy is a short trading approach when a decline is predicted for the following day, i.e., $\widehat{x}_t^{(c)} > \widehat{x}_{t+1}^{(c)}$. This strategy initiates by selling at $x_t^{(c)}$ to open the position and subsequently buying at $x_{t+1}^{(c)}$ to close the position, also with a holding period of 24:00 h. Despite their prevalence, these two strategies manifest three notable shortcomings. (1) Limited utilization of OHLC data information. The strategies do not fully capitalize the information embedded in the OHLC data, potentially resulting in missed profit opportunities. (2) Extended capital holding period. They have a long capital holding period, leading to inefficient capital utilization and increased holding risk. (3) Challenges in timely trading execution. In live trading scenarios, predicting $x_{t+1}^{(c)}$ often requires information from $x_t^{(c)}$. Therefore, these two strategies are often difficult to open a position with $x_t^{(c)}$ in a timely manner in actual trading.

The open-to-close (long) strategy and open-to-close (short) strategy represent trading approaches designed to leverage upward and downward market forecasts. Specifically, the open-to-close (long) strategy is implemented as a long position when predicting a bullish market for the subsequent day, i.e., $\widehat{x}_{t+1}^{(c)} > \widehat{x}_{t+1}^{(o)}$. It initiates by buying at $x_{t+1}^{(o)}$ to open the position and closes it by selling at $x_{t+1}^{(c)}$. On the other hand, the open-to-close (short) strategy is a short strategy engaged when a bearish market is predicted for the following day, i.e., $\widehat{x}_{t+1}^{(o)} > \widehat{x}_{t+1}^{(c)}$. It sells at $x_{t+1}^{(o)}$ to open the position and then buys at $x_{t+1}^{(c)}$ to close the position.

The open-to-high strategy, open-to-low strategy, low-to-close strategy, and high-to-close strategy integrate bullish and bearish judgments with low and high price forecasts. When a bullish market is predicted for the following day, i.e., $\widehat{x}_{t+1}^{(c)} > \widehat{x}_{t+1}^{(o)}$, the open price and close price are deemed to represent low and high levels, respectively. In this scenario, the open-to-high strategy involves opening a position at $x_{t+1}^{(o)}$ and closing it near $\widehat{x}_{t+1}^{(h)}$, while the low-to-close strategy is initiated by opening a position near $\widehat{x}_{t+1}^{(l)}$ and closed by selling at $x_{t+1}^{(c)}$. Conversely, when a bearish market is predicted for the following day, i.e., $\widehat{x}_{t+1}^{(o)} > \widehat{x}_{t+1}^{(c)}$, the open price and close price can be considered to be at high and low levels, respectively. In such case, the open-to-low strategy opens a position by selling at $x_{t+1}^{(o)}$ and closes it by buying near $\widehat{x}_{t+1}^{(l)}$, while the high-to-close strategy sells near $\widehat{x}_{t+1}^{(h)}$ to open a position and buys at $x_{t+1}^{(c)}$ to close it.

The low-to-high strategy is a trading strategy that leverages price prediction ranges. When $x_{t+1}^{(l)} \le \widehat{x}_{t+1}^{(l)}$ and $\widehat{x}_{t+1}^{(h)} \le x_{t+1}^{(h)}$, both low and high prices are triggered, and investors can firstly buy at $\widehat{x}_{t+1}^{(l)}$ to open a position and then sell at $\widehat{x}_{t+1}^{(h)}$ to close it, or investors can firstly sell at $\widehat{x}_{t+1}^{(h)}$ to open a position and then buy at $\widehat{x}_{t+1}^{(l)}$ to close it. When $x_{t+1}^{(l)} \le \widehat{x}_{t+1}^{(l)}$ and $x_{t+1}^{(h)} < \widehat{x}_{t+1}^{(h)}$, the low price is triggered but the high price is not, buy at $\widehat{x}_{t+1}^{(l)}$ to open a position and sell at $x_{t+1}^{(c)}$ to close it. When $\widehat{x}_{t+1}^{(l)} < x_{t+1}^{(l)}$ and $\widehat{x}_{t+1}^{(h)} \le x_{t+1}^{(h)}$, the high price is triggered but the low price is not, sell at $\widehat{x}_{t+1}^{(h)}$ to open a position and buy at $x_{t+1}^{(c)}$ to close it. And when $\widehat{x}_{t+1}^{(l)} < x_{t+1}^{(l)}$ and $x_{t+1}^{(h)} < \widehat{x}_{t+1}^{(h)}$, meaning neither the low nor high price is triggered, no trade is executed.

Various intraday trading strategies are designed to execute trades by buying at the predicted low price $\widehat{x}_{t+1}^{(l)}$ and selling at the anticipated high price $\widehat{x}_{t+1}^{(h)}$. However, an evident challenge is that the actual prices of

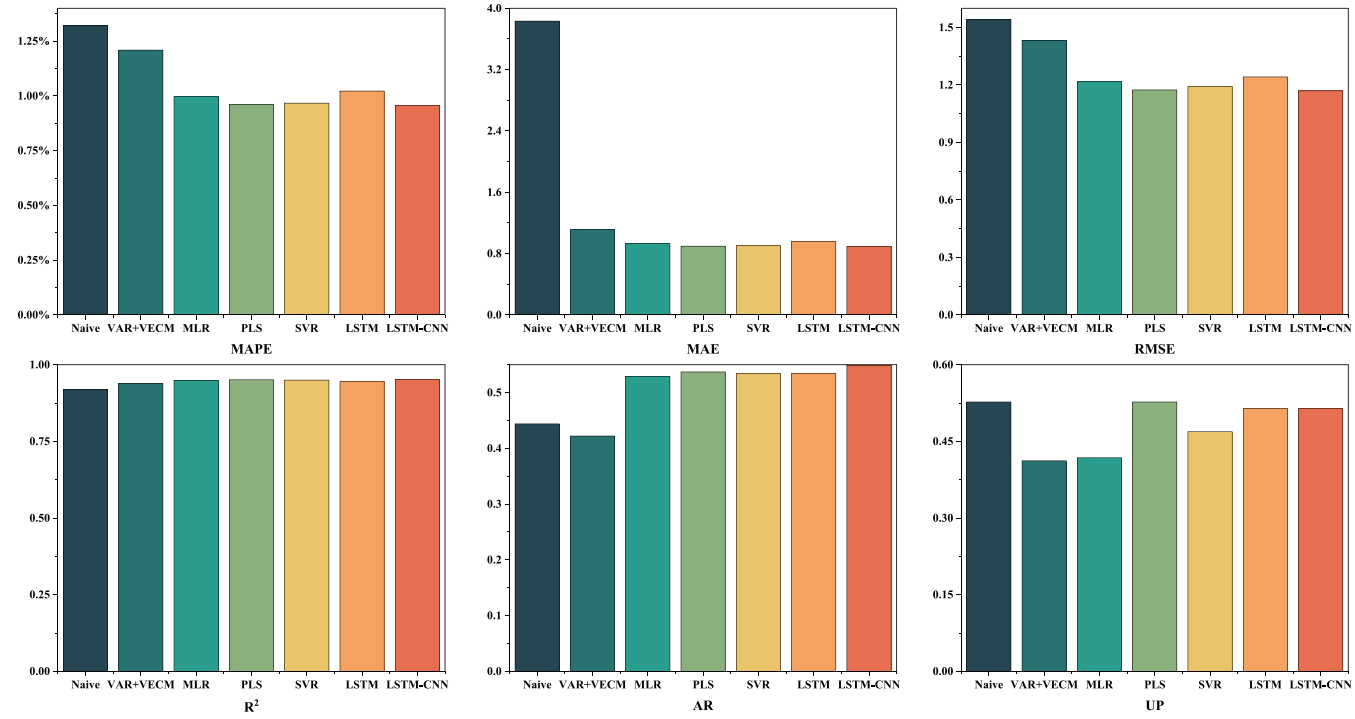

Fig. 8. Forecasting accuracy metrics for each model without using unconstrained transformation during EU ETS Phase IV.

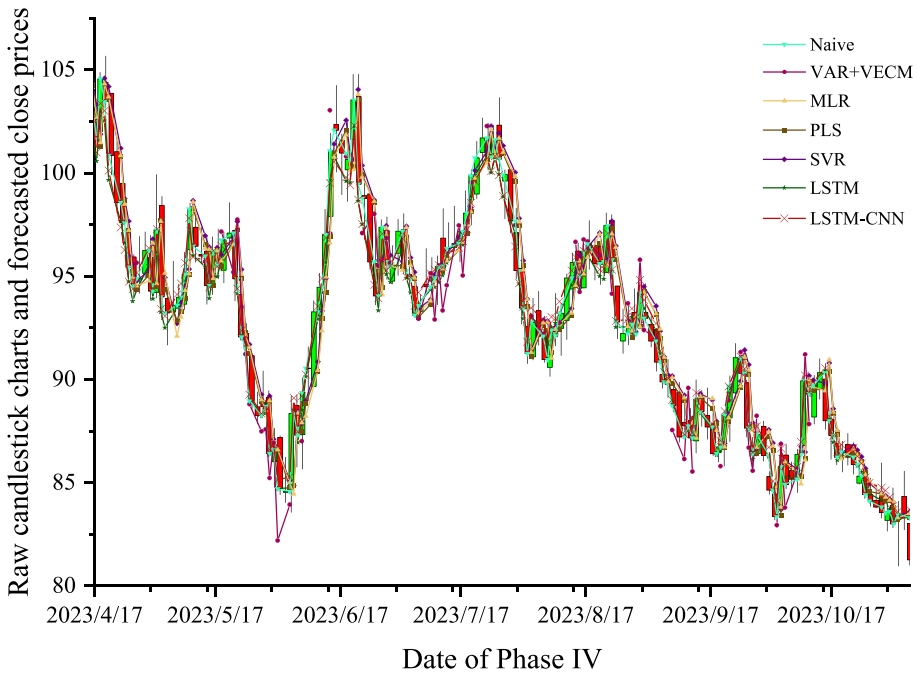

Fig. 9. Raw candlestick charts for EUA futures in EU ETS Phase IV and predicted close prices for each model without using unconstrained transformation.

Table 5
MAPE results of each model for EUA prices of different phases.

Models	Phase I	Phase II	Phase III	Phase IV
Naive method	12.772%	2.457%	2.043%	1.321%
VAR + VECM	20.088%	2.406%	1.883%	1.245%
MLR	12.605%	1.891%	1.675%	1.112%
PLS	12.605%	1.889%	1.675%	1.112%
SVR	12.399%	1.266%	1.557%	1.042%
LSTM	11.589%	1.254%	1.622%	1.015%
LSTM-CNN	11.035%	1.089%	1.499%	0.942%

Table 6
MAPE results of the LSTM-CNN in EU ETS Phase IV with penalty term-based loss function settings.

Penalty coefficient	Execution time	MAPE	Failure
100	Initial epoch	1.013%	3
200	Initial epoch	1.036%	3
500	Initial epoch	1.044%	0
1000	Initial epoch	1.048%	0
100	After 100 epochs	1.010%	0
200	After 100 epochs	1.032%	0
500	After 100 epochs	1.035%	0
1000	After 100 epochs	1.045%	0

EUA futures may not exactly match the predicted values, resulting in the strategies not being triggered. To address this, it becomes imperative to appropriately adjust the predicted price range, striking a balance between average return and overall return, with the goal of maximizing the overall return by triggering the strategy as frequently as possible. To achieve this balance, this study introduces two positive scaling factors, denoted as γ and δ. The adjusted low-high price range is $\left[\widehat{x}_{t+1}^{(l)^*}(1+\gamma), \widehat{x}_{t+1}^{(h)^*}(1-\delta)\right]$. For diverse intraday trading strategies, the optimal values for γ and δ are determined through back-testing, evaluating the overall return from historical data. In alignment with the principles of intraday trading, each strategy concludes its position at the market closing quotation when the scaled low or high price remains untriggered, as per the approach outlined by Huang et al. (2023a).

Table 7
Descriptions of trading strategies leveraging OHLC data.

Trading strategy	Trigger condition	Buying price	Selling price	Holding period
Close-to-close (long) strategy	$\widehat{x}_{t+1}^{(c)} > x_t^{(c)}$	$x_t^{(c)}$	$x_{t+1}^{(c)}$	24:00 h
Close-to-close (short) strategy	$x_t^{(c)} > \widehat{x}_{t+1}^{(c)}$	$x_{t+1}^{(c)}$	$x_t^{(c)}$	24:00 h
Open-to-close (long) strategy	$\widehat{x}_{t+1}^{(c)} > \widehat{x}_{t+1}^{(o)}$	$x_{t+1}^{(o)}$	$x_{t+1}^{(c)}$	10:00 h
Open-to-close (short) strategy	$\widehat{x}_{t+1}^{(o)} > \widehat{x}_{t+1}^{(c)}$	$x_{t+1}^{(c)}$	$x_{t+1}^{(o)}$	10:00 h
Open-to-high strategy	$\widehat{x}_{t+1}^{(c)} > \widehat{x}_{t+1}^{(o)}$ and $\widehat{x}_{t+1}^{(h)} \le x_{t+1}^{(h)}$	$x_{t+1}^{(o)}$	$\widehat{x}_{t+1}^{(h)}$	<10:00 h
Open-to-low strategy	$\widehat{x}_{t+1}^{(o)} > \widehat{x}_{t+1}^{(c)}$ and $x_{t+1}^{(l)} \le \widehat{x}_{t+1}^{(l)}$	$\widehat{x}_{t+1}^{(l)}$	$x_{t+1}^{(o)}$	<10:00 h
Low-to-close strategy	$\widehat{x}_{t+1}^{(c)} > \widehat{x}_{t+1}^{(o)}$ and $x_{t+1}^{(l)} \le \widehat{x}_{t+1}^{(l)}$	$\widehat{x}_{t+1}^{(l)}$	$x_{t+1}^{(c)}$	<10:00 h
High-to-close strategy	$\widehat{x}_{t+1}^{(o)} > \widehat{x}_{t+1}^{(c)}$ and $\widehat{x}_{t+1}^{(h)} \le x_{t+1}^{(h)}$	$x_{t+1}^{(c)}$	$\widehat{x}_{t+1}^{(h)}$	<10:00 h
Low-to-high strategy	$x_{t+1}^{(l)} \le \widehat{x}_{t+1}^{(l)}$ and $\widehat{x}_{t+1}^{(h)} \le x_{t+1}^{(h)}$	$\widehat{x}_{t+1}^{(l)}$	$\widehat{x}_{t+1}^{(h)}$	<10:00 h
	$x_{t+1}^{(l)} \le \widehat{x}_{t+1}^{(l)}$ and $x_{t+1}^{(h)} < \widehat{x}_{t+1}^{(h)}$	$\widehat{x}_{t+1}^{(l)}$	$\widehat{x}_{t+1}^{(c)}$	<10:00 h
	$\widehat{x}_{t+1}^{(l)} < x_{t+1}^{(l)}$ and $\widehat{x}_{t+1}^{(h)} \le x_{t+1}^{(h)}$	$\widehat{x}_{t+1}^{(c)}$	$\widehat{x}_{t+1}^{(h)}$	<10:00 h
	$\widehat{x}_{t+1}^{(l)} < x_{t+1}^{(l)}$ and $x_{t+1}^{(h)} < \widehat{x}_{t+1}^{(h)}$	No trade		<10:00 h

In assessing the return-on-investment (ROI) of the proposed intraday trading strategies within the actual EUA futures market, a set of evaluation metrics are selected in this study. Their specific formulas and meanings of these metrics are given below.

(1) The average return signifies the singular expected return achieved with each execution of the strategy.

$$\text{Average returns} = \bar{R} = \frac{1}{T}\sum_{t=1}^{T} R_t, \tag{27}$$

where T represents the total number of times the strategy is executed; R_t denotes the individual return obtained when the strategy is triggered at period t. Factoring in margin rate and transaction fee, R_t is calculated using the formula:

$$R_t = \frac{(CP_t - OP_t) \times Lot - Fee}{OP_t \times Lot \times Margin} \times 100\%, \tag{28}$$

where OP_t and CP_t denote the opening price and closing price at period t, respectively. *Lot* equals to 1000 since one lot of EUA futures corresponds to 1000 EUAs, where each EUA is an allowance with the right to emit one ton of CO_2 equivalent. As for *Fee*, according to ICE's charging rules, the exchange fee for each lot of EUA futures is 3.00 USD and the clearing fee is 7.00 USD, for a total of 10.00 USD per lot.[1] Concerning the *Margin*, the margin rate for EUA futures fluctuates over time, with this study adopting an intermediate value of 10%.[2]

(2) The standard deviation of returns quantifies the volatility of individual returns achieved by a strategy through multiple executions and is calculated as:

$$\text{Standard deviation of returns} = sd = \frac{1}{T-1}\sum_{t=1}^{T}(R_t - \bar{R})^2. \tag{29}$$

(3) The annualized rate of return (ARR) is a theoretical return rate derived by converting the return rate achieved during the testing period into an annualized rate. The calculation formula for ARR is:

$$\text{ARR} = \left[\left(\prod_{t=1}^{T}(1+R_t)\right)^{\frac{258}{TD}} - 1\right], \tag{30}$$

where $\prod_{t=1}^{T}(1+R_t)$ denotes the cumulative return rate over the test period, and in this study, it is assumed that a full position is established each time the strategy is executed. The value 258 corresponds to the number of trading days in a year of the EU ETS. And *TD* refers to the number of timestamps included in the test period.

(4) The Sharpe Ratio serves to quantify the excess reward generated by a trading strategy relative to each unit of total risk it incurs. A Sharpe Ratio exceeding 1 indicates that the trading strategy's reward surpasses the volatility risk. The formula for computing the Sharpe Ratio is as follows:

$$\text{Sharpe Ratio} = \frac{ARR - R_f}{sd \times T \times 258/TD}, \tag{31}$$

where R_f represents the annualized risk-free rate, set as the ten-year treasury yield of America on November 1, 2023, which stands at 4.6230%.

(5) Maximum drawdown is the percentage by which a trading strategy's cumulative return over the entire test period falls from its historical peak to its historical trough. It is calculated using the following formula:

$$\text{Maximum Drawdown} = MD_T = \max_{t_1,t_2\in(1,T)}\left(\frac{\text{CR}_{t1} - CR_{t2}}{\text{CR}_{t1}}\right), \tag{32}$$

where CR_t denotes the cumulative return rate at period t, and $t_1 < t_2$.

6.5. Performance of intraday trading strategies in EU ETS Phase IV

Utilizing the out-of-sample prediction results from LSTM-CNN, this study delves into the actual investment performance of the proposed trading strategy employing OHLC data for EUA futures trading in Phase IV of the EU ETS. The results are outlined in Table 8. Among them, the open-to-high strategy yields optimal results with a $\delta = 0.92\%$, the open-to-low strategy is optimal with $\gamma = 0.19\%$, open-to-high strategy + open-to-low strategy is optimal with $\gamma = 0.19\%$ and $\delta = 0.92\%$, low-to-close strategy is optimal with $\delta = 0.18\%$, high-to-close strategy is optimal with $\gamma = 0.74\%$, low-to-close strategy + high-to-close strategy is optimal with $\gamma = 0.74\%$ and $\delta = 0.18\%$, and low-to-high strategy is optimal with $\gamma = 1.01\%$ and $\delta = 0.19\%$.

Several noteworthy conclusions can be derived: (1) Concerning average returns (RMEAN), the top three highest are the open-to-low strategy (8.258%), high-to-close strategy (8.231%), and open-to-close (short) strategy (7.185%). These strategies excel due to their fewer triggers, coupled with a substantial return on investment per trigger. (2) Regarding the annualized rate of return (ARR) and Sharpe ratio, the top three highest are the low-to-high strategy (2887.956 and 80.313), open-to-low strategy (104.846 and 9.429), and open-to-close (short) strategy (47.610 and 4.004). The outstanding performance of these strategies can

Table 8
Investment performance of various intraday trading strategies in EU ETS Phase IV based on out-of-sample forecasts with LSTM-CNN.

Trading strategy	Triggered number	RMEAN	RSD	ARR	Sharpe	MD
close-to-close (long) strategy	90	−0.403%	0.158	−0.925	−0.039	0.861
close-to-close (short) strategy	55	3.461%	0.183	4.459	0.249	0.729
close-to-close strategy	145	1.063%	0.168	−0.591	−0.015	0.868
open-to-close (long) strategy	107	−0.090%	0.155	−0.906	−0.033	0.830
open-to-close (short) strategy	39	7.185%	0.172	47.610	4.004	0.466
open-to-close strategy	146	1.853%	0.162	3.551	0.084	0.807
open-to-high strategy	107	1.373%	0.097	4.317	0.234	0.503
open-to-low strategy	39	8.258%	0.161	104.846	9.429	0.445
open-to-high strategy + open-to-low strategy	146	3.212%	0.121	561.739	18.035	0.480
low-to-close strategy	49	4.704%	0.145	24.356	1.939	0.326
high-to-close strategy	28	8.231%	0.194	21.526	2.243	0.408
low-to-close strategy + high-to-close strategy	77	5.986%	0.164	570.169	25.574	0.354
low-to-high strategy	137	4.464%	0.149	2887.956	80.313	0.713

[1] ICE fee rules website: https://www.ice.com/publicdocs/IFEU_Exchange_Clearing_Fees.pdf.

[2] ICE EUA futures introduction website: https://www.ice.com/products/197/EUA-Futures.

be attributed to a relatively high number of strategy triggers, substantial average returns, and the compounding effect amplifying the ARR. (3) In terms of maximum retracement (MD), the low-to-close strategy (0.326), the open-to-low strategy (0.445), and the open-to-close (short) strategy (0.466) are the three lowest trading strategies. (4) Two combined trading strategies, namely, the open-to-high strategy + open-to-low strategy and the low-to-close strategy + high-to-close strategy, show good investment returns. These strategies yield average returns of 3.212% and 5.986%, with corresponding Sharpe ratios of 18.035 and 25.574, respectively. (5) Overall, the proposed intraday trading strategies based on OHLC data exhibit significantly superior returns compared to the conventional close-to-close (long) strategy relying solely on close prices. This underscores a considerable investment potential of the proposed intraday trading strategies within the EUA futures market.

7. Conclusion

As the EU's flagship carbon reduction policy, the EU ETS has played a key role in reducing carbon emissions in the EU's electricity, industry, and aviation sectors over the past two decades. Functioning as the "currency of circulation" within the framework of the EU ETS, EUA futures magnetically draw an extensive cohort of global speculators. Accurate forecasts of EUA futures prices prove to be of paramount significance for speculators to adjust their portfolios and generate returns, thus injecting good liquidity and price discovery into the EUA futures market. Moreover, the accurate forecasting of EUA futures prices serves a dual purpose by empowering regulated enterprises to hedge production risks through virtual inventories, while concurrently providing policymakers with a standard to assess the efficacy of the EU ETS. The modeling framework expounded in this study holds the potential for diverse ETSs worldwide, thereby fostering a more unified and concerted effort towards mitigating greenhouse gas emissions on a global scale.

This study advances a model-driven LSTM-CNN hybrid model, adept in extracting and integrating numerical data attributes and candlestick chart features. The objective is to attain precise and unbiased structural forecasting of EUA futures OHLC prices throughout the distinctive phases of the EU ETS. This study enriches the structural modeling approach for complex data and proposes fruitful intraday trading strategies based on the structural forecasts of OHLC data. The overarching intent of the proposed intraday trading strategies is to provide speculators with a strategic advantage in enhancing their prospects for superior investment returns within the dynamic landscape of financial markets. In addition, this study conducts a comprehensive examination into the temporal dimensions of the long-term modeling window, spanning across the four phases of the EU ETS from 2005 to 2023. This dual-temporal perspective not only provides a historical lens through which to comprehend the evolution of the EU ETS but also offers a forward-looking vantage point.

Based on the modeling results of EUA futures, the main conclusions drawn from this study are as follows.

(1) Firstly, based on the unconstrained transformation and model-driven loss function settings, ANNs achieve accurate structural prediction of OHLC prices for EUA futures in Phase IV of the EU ETS, in which the hybrid model of LSTM-CNN is the most powerful in terms of prediction ability. The LSTM-CNN obtains a MAPE of 0.942%, a MAE of 0.877, an RMSE of 1.157, an R^2 of 0.953, an AR of 0.544, and an UP of 0.579. Furthermore, the unconstrained transformation not only ensures the structural forecasting of OHLC data but also improves the forecasting accuracy of ANNs. This augmentation is posited on the premise that the unconstrained transformation facilitates effective artificial feature extraction within the ANN architecture.

(2) Secondly, the forecasting accuracy of the advanced LSTM-CNN model manifests robustness across the distinctive phases of the EU ETS. Notably, its MAPE outcomes surpass those of other econometric and machine learning models. Specifically, in relation to the average MAPE across each phase of the EU ETS, the LSTM-CNN model exhibits marked enhancements—improving by 21.66%, 43.15%, 15.73%, 15.72%, 10.45%, and 5.91% in comparison to the Naive method, VAR + VECM, MLR, PLS, SVR, and LSTM, respectively.

(3) Thirdly, the proposed intraday trading strategies leveraging OHLC data have yielded substantially superior returns compared to the conventional close-to-close strategy anchored solely on close price. This substantiates the considerable investment potential of the energy futures market. The best-performing trading strategy appears to be the low-to-high strategy, which is consistent with the empirical findings of Huang et al. (2022a, 2023a). In the live trading scenario of EU ETS Phase IV, the low-to-high strategy, based on the LSTM-CNN out-of-sample prediction results, obtained an average return of 4.464%, a standard deviation of return at 0.149, an annualized return of 2887.956, a Sharpe ratio of 80.313, and a maximum retracement of 0.713. Besides, speculators may also consider two combination trading strategies, i.e., open-to-high strategy + open-to-low strategy and low-to-close strategy + high-to-close strategy. This combination of strategies has more triggering opportunities, allowing speculators to achieve substantial returns through the power of compounding.

In forthcoming research endeavors, the integration of textual data features stands out as a promising avenue to augment the predictive accuracy of EUA futures prices. As behavioral finance theory research has shown, investor attention and emotions exert a significant influence on price fluctuations within financial markets (Dolan, 2002). The textual data influencing EUA prices may encompass the policy changes in carbon regulation (Benz and Trück, 2009), and search history for Google Trends (Pan et al., 2023). Additionally, another interesting direction for further exploration lies in the simultaneous incorporation of data at various temporal frequencies. For instance, using hourly candlestick charts, and minute-by-minute or tick-by-tick historical EUA futures prices as the input of ANNs. The utilization of finer time granularity data can improve the overall accuracy and efficacy of the forecasting modeling as it encapsulates more trading information (Selvamuthu et al., 2019).

CRediT authorship contribution statement

Wenyang Huang: Writing – review & editing, Writing – original draft, Visualization, Software, Methodology, Formal analysis, Data curation. **Jianyu Zhao:** Writing – original draft, Software, Methodology. **Xiaokang Wang:** Writing – review & editing, Supervision, Funding acquisition, Formal analysis, Conceptualization.

Acknowledgements

The authors are grateful for the financial support from the Beijing Natural Science Foundation (Grant No. 9244030), Youth Project of MOE (Ministry of Education) Foundation on Humanities and Social Sciences (Grant No. 23YJCZH223), and Fundamental Research Funds for the Central Universities (Grant No. 2023RC11). Besides, the authors also thank the anonymous reviewers for insightful comments that helped us improve the quality of the paper.

Appendix A. Supplementary data

Supplementary data to this article can be found online at https://doi.org/10.1016/j.eneco.2024.107459.

References

Aatola, P., Ollikainen, M., Toppinen, A., 2013. Price determination in the EU ETS market: theory and econometric analysis with market fundamentals. Energy Econ. 36, 380–395.

Abrell, J., Ndoye, F.A., Zachmann, G., 2011. Assessing the impact of the EU ETS using firm level data. Bruegel working paper.

Alberola, E., Chevallier, J., Ch'eze, B., 2008. Price drivers and structural breaks in European carbon prices 2005–07. Energy Policy 36, 787–797.

Batten, J.A., Maddox, G.E., Young, M.R., 2020. Does weather, or energy prices, affect carbon prices? Energy Econ. 105016.
Bayer, P., Aklin, M., 2020. The European Union emissions trading system reduced CO_2 emissions despite low prices. Proc. Natl. Acad. Sci. 117 (16), 8804–8812, 2020.
Benz, E., Trück, S., 2009. Modeling the price dynamics of CO2 emission allowances. Energy Econ. 31 (1), 4–15.
Bruninx, K., Ovaere, M., Delarue, E., 2020. The long-term impact of the market stability reserve on the EU emission trading system. Energy Econ. 89, 104746.
Byun, S.J., Cho, H., 2013. Forecasting carbon futures volatility using GARCH models with energy volatilities. Energy Econ. 40, 207–221.
Caginalp, G., Laurent, H., 1998. The predictive power of price patterns. Appl. Math. Finan. 5 (3–4), 181–205.
Cagliero, L., Fior, J., Garza, P., 2023. Shortlisting machine learning-based stock trading recommendations using candlestick pattern recognition. Expert Syst. Appl. 216, 119493.
Chen, J.H., Tsai, Y.C., 2020. Encoding candlesticks as images for pattern classification using convolutional neural networks. Finan. Innov. 6 (1), 1–19.
Chen, S., Bao, S., Zhou, Y., 2016. The predictive power of Japanese candlestick charting in Chinese stock market. Physica A: Stat. Mech. Appl. 457, 148–165.
Chen, J., Wen, Y., Nanehkaran, Y.A., et al., 2023. Machine learning techniques for stock price prediction and graphic signal recognition. Eng. Appl. Artif. Intell. 121, 106038.
Chevallier, J., 2009. Carbon futures and macroeconomic risk factors: a view from the EU ETS. Energy Econ. 31, 614–625.
Chevallier, J., 2010. Volatility forecasting of carbon prices using factor models. Econ. Bull. 30 (2), 1642–1660.
Chevallier, J., 2011. A model of carbon price interactions with macroeconomic and energy dynamics. Energy Econ. 33 (6), 1295–1312.
Chevallier, J., Sévi, B., 2011. On the realized volatility of the ECX CO2 emissions 2008 futures contract: distribution, dynamics and forecasting. Ann. Finance 7, 1–29.
Convery, F.J., 2009. Origins and development of the EU ETS. Environ. Resour. Econ. 43, 391–412.
Cooper, M.J., Cliff, M.T., Gulen, H., 2008. Return differences between trading and non-trading hours: Like night and day. Available at SSRN 1004081.
Creti, A., Joets, M., 2017. Multiple bubbles in the European union emission trading scheme. Energy Policy 107, 119–130.
Creti, A., Jouvet, P.A., Mignon, V., 2012. Carbon price drivers: Phase I versus phase II equilibrium? Energy Econ. 34, 327–334.
Dai, X., Xiao, L., Wang, Q., et al., 2021. Multiscale interplay of higher-order moments between the carbon and energy markets during Phase III of the EU ETS. Energy Policy 156, 112428.
De Perthuis, C., Trotignon, R., 2014. Governance of CO2 markets: lessons from the EU ETS. Energy Policy 75, 100–106.
Dhamija, A.K., Yadav, S.S., Jain, P.K., 2017. Forecasting volatility of carbon under EU ETS: a multi-phase study. Environ. Econ. Policy Stud. 19 (2), 299–335.
Dolan, R.J., 2002. Emotion, cognition, and behavior. Science 298 (5596), 1191–1194.
Dunis, C.L., Laws, J., Rudy, J., 2011. Profitable mean reversion after large price drops: a story of day and night in the S&P 500, 400 MidCap and 600 SmallCap indices. J. Asset Manag. 12, 185–202.
Ellerman, A.D., Marcantonini, C., Zaklan, A., 2016. The European Union emissions trading system: ten years and counting. Rev. Environ. Econ. Policy 10 (1), 89–107.
European Commission, 2022. Climate Action Progress Report 2022. Retrieved from. https://climate.ec.europa.eu/system/files/2022-12/com_2022_514_web_en.pdf.
European Commission, 2023. Phase 1 and 2 (2005–2012). Retrieved from. https://ec.europa.eu/clima/policies/ets/pre2013_en#tab-0-0.
Fan, X., Li, S., Tian, L., 2015. Chaotic characteristic identification for carbon price and an multi-layer perceptron network prediction model. Expert Syst. Appl. 42 (8), 3945–3952.
Flachsland, C., Pahle, M., Burtraw, D., et al., 2020. How to avoid history repeating itself: the case for an EU emissions trading system (EU ETS) price floor revisited. Clim. Pol. 20 (1), 133–142.
García, A., Jaramillo-Morán, M.A., 2020. Short-term European Union allowance price forecasting with artificial neural networks. Entrepr. Sustain. Issues 8 (1), 261.
García-Martos, C., Rodríguez, J., Sánchez, M.J., 2013. Modelling and forecasting fossil fuels, CO2 and electricity prices and their volatilities. Appl. Energy 101, 363–375.
Gong, X., Li, M., Guan, K., et al., 2023. Climate change attention and carbon futures return prediction. J. Futur. Mark. 43 (9), 1261–1288.
Goo, Y., Chen, D., Chang, Y., 2007. The application of Japanese candlestick trading strategies in Taiwan. Invest. Manag. Finan. Innov. 4, 49–79.
Graves, A., Schmidhuber, J., 2005. Framewise phoneme classification with bidirectional LSTMand other neural network architectures. Neural Netw. 18 (5–6), 602–610.
Gu, L., Peng, Y., Vigne, S.A., Wang, Y., 2023. Hidden costs of non-green performance? The impact of air pollution awareness on loan rates for Chinese firms. J. Econ. Behav. Organ. 213, 233–250.
Guðbrandsdóttir, H.N., Haraldsson, H.Ó., 2011. Predicting the price of EU ETS carbon credits. Syst. Eng. Proc. 1, 481–489.
Hammoudeh, S., Nguyen, D.K., Sousa, R.M., 2014. What explain the short-term dynamics of the prices of CO_2 emissions? Energy Econ. 46, 22–135.
Hepburn, C., Grubb, M., Neuhoff, K., et al., 2006. Auctioning of EU ETS phase II allowances: how and why? Clim. Pol. 6 (1), 137–160.
Hickmann, T., 2014. Science–policy interaction in international environmental politics: an analysis of the ozone regime and the climate regime. Environ. Econ. Policy Stud. 16, 21–44.
Hintermann, B., 2010. Allowance price drivers in the first phase of the EU ETS. J. Environ. Econ. Manag. 59 (1), 43–56.
Hintermann, B., Peterson, S., Rickels, W., 2016. Price and market behavior in phase II of the EU ETS: a review of the literature. Rev. Environ. Econ. Policy 10 (1), 108–128.
Hoseinzade, E., Haratizadeh, S., 2019. CNNpred: CNN-based stock market prediction using a diverse set of variables. Expert Syst. Appl. 129, 273–285.
Hu, J., Crijns-Graus, W., Lam, L., et al., 2015. Ex-ante evaluation of EU ETS during 2013–2030: EU-internal abatement. Energy Policy 77, 152–163.
Huang, T., Saporta, G., Wang, H., et al., 2021a. A robust spatial autoregressive scalar on function regression with t distribution. ADAC 15 (1), 57–81.
Hu, C., He, L.T., 2007. An application of interval methods to stock market forecasting. Reliable Computing 13 (5), 423–434.
Huang, Y., Dai, X., Wang, Q., et al., 2021b. A hybrid model for carbon price forecasting using GARCH and long short-term memory network. Appl. Energy 285, 116485.
Huang, W., Wang, H., Qin, H., et al., 2022a. Convolutional neural network forecasting of European Union allowances futures using a novel unconstrained transformation method. Energy Econ. 110, 106049.
Huang, W., Wang, H., Wang, S., 2022b. A pseudo principal component analysis method for multi-dimensional open-high-low-close data in candlestick chart. Commun. Stat. Theory Methods 1–27.
Huang, W., Gao, T., Hao, Y., et al., 2023a. Transformer-based forecasting for intraday trading in the Shanghai crude oil market: analyzing open-high-low-close prices. Energy Econ. 127, 107106.
Huang, W., Wang, H., Wang, S., 2024b. A structural VAR and VECM modeling method for open-high-low-close data contained in candlestick chart. Financ. Innov. 10, 97. https://link.springer.com/article/10.1186/s40854-024-00622-6.
Huang, W., Wang, H., Wei, Y., 2023b. Identifying the determinants of European carbon allowances prices: a novel robust partial least squares method for open-high-low-close data. Int. Rev. Financ. Anal. 90, 102938.
Huang, W., Wang, H., Wei, Y., et al., 2024a. Complex network analysis of global stock market co-movement during the COVID-19 pandemic based on intraday open-high-low-close data. Financ. Innov. 10 (1), 7. https://link.springer.com/article/10.1186/s40854-023-00548-5.
Hung, C.C., Chen, Y.J., 2021. DPP: deep predictor for price movement from candlestick charts. PLoS One 16 (6), e0252404.
Hung, C.C., Chen, Y.J., Guo, S.J., et al., 2020. Predicting the price movement from candlestick charts: a CNN-based approach. Int. J. Ad Hoc Ubiquitous Comput. 34 (2), 111–120.
Jeszke, R., Lizak, S., 2021. Reflections on the mechanisms to protect against formation of price bubble in the EU ETS market. Environ. Protect. Nat. Resourc. 32 (2), 8–17.
Ji, L., Zou, Y., He, K., et al., 2019. Carbon futures price forecasting based with ARIMA-CNN-LSTM model. Proc. Comput. Sci. 162, 33–38.
Jiang, J., Kelly, B.T., Xiu, D., 2023. (Re-) Imag (in) ing price trends. The Journal of Finance 78 (6), 3193–3249.
Kelly, M.A., Clark, S.P., 2011. Returns in trading versus non-trading hours: the difference is day and night. J. Asset Manag. 12, 132–145.
Kim, T., Kim, H.Y., 2019. Forecasting stock prices with a feature fusion LSTM-CNN model using different representations of the same data. PLoS One 14 (2), e0212320.
Kim, J., Park, Y.J., Ryu, D., 2017. Stochastic volatility of the futures prices of emission allowances: a Bayesian approach. Physica A: Stat. Mech. Appl. 465, 714–724.
Koch, N., Fuss, S., Grosjean, G., Edenhofer, O., 2014. Causes of the EU ETS price drop: recession, CDM, renewable policies or a bit of everything?—new evidence. Energy Policy 73, 676–685.
Kossoy, A., Guigon, P., 2012. State and trends of the carbon market, 2012.
Laing, T., Sato, M., Grubb, M., et al., 2013. Assessing the Effectiveness of the EU Emissions Trading System. Grantham Research Institute on Climate Change and the Environment, London.
Lepone, A., Rahman, R.T., Yang, J.Y., 2011. The Impact of European Union Emissions Trading Scheme (EU ETS) National Allocation Plans (NAP) on carbon markets. Low Carbon Econ. 2 (02), 71.
Li, C.Y., Chen, S.N., Lin, S.K., 2016. Pricing derivatives with modeling CO_2 emission allowance using a regime-switching jump diffusion model: with regime-switching risk premium. Eur. J. Financ. 22 (10), 887–908.
Li, H., Jin, F., Sun, S., et al., 2021. A new secondary decomposition ensemble learning approach for carbon price forecasting. Knowl.-Based Syst. 214, 106686.
Li, D., Li, Y., Wang, C., et al., 2023. Forecasting carbon prices based on real-time decomposition and causal temporal convolutional networks. Appl. Energy 331, 120452.
Liang, M., Wu, S., Wang, X., et al., 2022. A stock time series forecasting approach incorporating candlestick patterns and sequence similarity. Expert Syst. Appl. 205, 117595.
Liu, H., Shen, L., 2020. Forecasting carbon price using empirical wavelet transform and gated recurrent unit neural network. Carbon Manag. 11 (1), 25–37.
Liu, X., An, H., Wang, L., et al., 2017. An integrated approach to optimize moving average rules in the EUA futures market based on particle swarm optimization and genetic algorithms. Appl. Energy 185, 1778–1787.
Lu, W., Wang, W.J., 2011. An investigation into the evolved relationship between spot and futures in the European Union emission trading scheme. Int. J. Green Econ. 5 (2), 133–142.
Lu, T.H., Shiu, Y.M., Liu, T.C., 2012. Profitable candlestick trading strategies—the evidence from a new perspective. Rev. Financ. Econ., 21(2), 0–68. https://www.sciencedirect.com/science/article/pii/S1058330012000092.
Lu, W., Li, J., Wang, J., et al., 2021. A CNN-BiLSTM-AM method for stock price prediction. Neural Comput. & Applic. 33, 4741–4753.
Lucia, J.J., Mansanet-Bataller, M., Pardo, Á., 2015. Speculative and hedging activities in the European carbon market. Energy Policy 82, 342–351.
Lutz, B.J., Pigorsch, U., Rotfuß, W., 2013. Nonlinearity in cap-and-trade systems: the EUA price and its fundamentals. Energy Econ. 40, 222–232.
Lv, T., Hao, Y., 2017. Further analysis of candlestick Patterns' predictive power. In: Data Science: Third International Conference of Pioneering Computer Scientists,

Engineers and Educators, ICPCSEE 2017, Changsha, China, September 22–24, 2017, Proceedings, Part I. Springer Singapore, pp. 73–87.
Ma, F., Cao, J., Wang, Y., et al., 2023. Dissecting climate change risk and financial market instability: Implications for ecological risk management. Risk Analysis, 1-27.
Meadows, D., Vis, P., Zapfel, P., 2019. The EU emissions trading system. In: Towards a Climate-Neutral Europe, pp. 66–94.
Mirzaee Ghazani, M., Jafari, M.A., 2021. The efficiency of CO_2 market in the phase III EU ETS: analyzing in the context of a dynamic approach. Environ. Sci. Pollut. Res. 28 (43), 61080–61095.
Nadirgil, O., 2023. Carbon price prediction using multiple hybrid machine learning models optimized by genetic algorithm. J. Environ. Manag. 342, 118061.
Needham, T., 1993. A visual explanation of Jensen's inequality. Am. Math. Mon. 100 (8), 768–771.
Neuhoff, K., Åhman, M., Betz, R., et al., 2006. Implications of announced phase II national allocation plans for the EU ETS. Clim. Pol. 6 (4), 411–422.
Nison, S., 1994. Beyond Candlesticks: New Japanese Charting Techniques Revealed. John Wiley & Sons.
Nison, S., 2001. Japanese Candlestick Charting Techniques: A Contemporary Guide to the Ancient Investment Techniques of the Far East. Penguin.
Pan, D., Zhang, C., Zhu, D., et al., 2023. Carbon price forecasting based on news text mining considering investor attention. Environ. Sci. Pollut. Res. 30 (11), 28704–28717.
Paolella, M.S., Taschini, L., 2008. An econometric analysis of emission allowance prices. J. Bank. Financ. 32 (10), 2022–2032.
Pawłowski, P., 2021. Carbon Emissions Futures Price Forecasting with Random Forest. Rynek Energii.
Perino, G., 2018. New EU ETS phase 4 rules temporarily puncture waterbed. Nat. Clim. Chang. 8 (4), 262–264.
Qin, Q., Huang, Z., Zhou, Z., et al., 2022. Hodrick–Prescott filter-based hybrid ARIMA–SLFNs model with residual decomposition scheme for carbon price forecasting. Appl. Soft Comput. 119, 108560.
Rannou, Y., Boutabba, M.A., Barneto, P., 2021. Are Green Bond and Carbon Markets in Europe complements or substitutes? Insights from the activity of power firms. Energy Econ. 104, 105651.
Reboredo, J.C., 2013. Modeling EU allowances and oil market interdependence. Implications for portfolio management. Energy Econ. 36, 471–480.
Rostamian, A., O'Hara, J.G., 2022. Event prediction within directional change framework using a CNN-LSTM model. Neural Comput. & Applic. 34 (20), 17193–17205.
Santur, Y., 2022. Candlestick chart based trading system using ensemble learning for financial assets. Sigma J. Eng. Nat. Sci. 40 (2), 370–379.
Sartor, O., Pallière, C., Lecourt, S., 2014. Benchmark-based allocations in EU ETS Phase 3: an early assessment. Clim. Pol. 14 (4), 507–524.
Sato, M., Rafaty, R., Calel, R., et al., 2022. Allocation, allocation, allocation! The political economy of the development of the European Union emissions trading system. Wiley Interdiscip. Rev. Clim. Chang. 13 (5), e796.
Selvamuthu, D., Kumar, V., Mishra, A., 2019. Indian stock market prediction using artificial neural networks on tick data. Finan. Innov. 5 (1), 1–12.
Sheng, C., Wang, G., Geng, Y., et al., 2020. The correlation analysis of futures pricing mechanism in China's carbon financial market. Sustainability 12 (18), 7317.
Sherstinsky, A., 2020. Fundamentals of recurrent neural network (RNN) and long short-term memory (LSTM) network. Physica D: Nonlinear Phenomena 404, 132306.
Shin, H.G., Ra, I., Choi, Y.H., 2019. A deep multimodal reinforcement learning system combined with CNN and LSTM for stock trading. In: International Conference on Information and Communication Technology Convergence (ICTC). IEEE, pp. 7–11.
Skjærseth, J.B., Wettestad, J., 2009. The origin, evolution and consequences of the EU emissions trading system. Glob. Environ. Polit. 9 (2), 101–122.
Sun, G.Q., Che, T., Wei, Z.N., et al., 2016. A carbon price forecasting model based on variational mode decomposition and spiking neural networks. Energies 9 (1), 54.
Tan, X.P., Wang, X.Y., 2017. Dependence changes between the carbon price and its fundamentals: a quantile regression approach. Appl. Energy 190, 306–325.
Tsai, M.T., Kuo, Y.T., 2014. Application of radial basis function neural network for carbon price forecasting. Appl. Mech. Mater. 590, 683–687. Trans Tech Publications Ltd.
Tsai, C.F., Quan, Z.Y., 2014. Stock prediction by searching for similarities in candlestick charts. ACM Trans. Manag. Inf. Syst. 5 (2), 1–21.
Varadharajan, P., Vikkraman, P., 2011. Effectiveness of technical analysis using candlestick chart for selection of equity stock in Indian capital market. J. Contemp. Manag. Res. 5 (1).
Viteva, S., Veld-Merkoulova, Y.V., Campbell, K., 2014. The forecasting accuracy of implied volatility from ECX carbon options. Energy Econ. 45, 475–484.
von Mettenheim, H.J., Breitner, M.H., 2012. Forecasting and trading the high-low range of stocks and ETFs with Neural Networks. Engineering Applications of Neural Networks: 13th International Conference, EANN 2012, London, UK, September 20–23. Proceedings 13. Springer Berlin Heidelberg, pp. 423–432.
Wang, Y., Lucey, B.M., Vigne, S.A., et al., 2022a. The effects of central bank digital currencies news on financial markets. Technol. Forecast. Soc. Change. 180, 121715.
Wang, Y., 2022. Volatility spillovers across NFTs news attention and financial markets. Int. Rev. Financ. Anal. 83, 102313.
Wang, H., Huang, T., Wang, S., 2021a. A flexible spatial autoregressive modelling framework for mixed covariates of multiple data types. Commun. Stat. Simul. Comput. 50 (11), 3498–3515.
Wang, H., Wang, J., Cao, L., et al., 2021b. A stock closing price prediction model based on CNN-BiSLSTM. Complexity 1–12.
Wang, Y., Wei, Y., Lucey, B.M., et al., 2023. Return spillover analysis across central bank digital currency attention and cryptocurrency markets. Res. Int. Bus. Finance 64, 101896.
Wang, M., Zhu, M., Tian, L., 2022b. A novel framework for carbon price forecasting with uncertainties. Energy Econ. 106162.
Wei, Y., Gong, P., Zhang, J., et al., 2021. Exploring public opinions on climate change policy in "Big Data Era"—A case study of the European Union Emission Trading System (EU-ETS) based on Twitter. Energy Policy 158, 112559.
Wei, Y., Li, Y., Wang, Z., 2022. Multiple price bubbles in global major emission trading schemes: Evidence from European Union, New Zealand, South Korea and China. Energy Econ. 113, 106232.
Wei, Y., Zhang, J., Bai, L., et al., 2023. Connectedness among El Niño-Southern Oscillation, carbon emission allowance, crude oil and renewable energy stock markets: Time-and frequency-domain evidence based on TVP-VAR model. Renew. Energy 202, 289–309.
Wu, J.M.T., Li, Z., Herencsar, N., et al., 2021. A graph-based CNN-LSTM stock price prediction algorithm with leading indicators. Multimedia Systems 1–20.
Wu, M., Li, K.X., Xiao, Y., et al., 2022. Carbon emission trading scheme in the shipping sector: drivers, challenges, and impacts. Mar. Policy 138, 104989.
Xu, H., Wang, M., Jiang, S., et al., 2020. Carbon price forecasting with complex network and extreme learning machine. Physica A: Stat. Mech. Appl. 545, 122830.
Yu, Y., Si, X., Hu, C., et al., 2019. A review of recurrent neural networks: LSTM cells and network architectures. Neural Comput. 31 (7), 1235–1270.
Yun, P., Zhang, C., Wu, Y., et al., 2022. Forecasting carbon dioxide price using a time-varying high-order moment hybrid model of NAGARCHSK and gated recurrent unit network. Int. J. Environ. Res. Public Health 19 (2), 899.
Yun, P., Huang, X., Wu, Y., et al., 2023. Forecasting carbon dioxide emission price using a novel mode decomposition machine learning hybrid model of CEEMDAN-LSTM. Energy Sci. Eng. 11 (1), 79–96.
Zhang, D., Tang, P., 2023a. Forecasting European Union allowances futures: the role of technical indicators. Energy 270, 126916.
Zhang, T., Tang, Z., 2023b. Multi-step carbon price forecasting based on a new quadratic decomposition ensemble learning approach. Front. Energy Res. 10, 991570.
Zhang, D., Wang, C., Wang, Y., 2024. Unveiling the critical nexus: Volatility of crude oil future prices and trade partner's cash holding behavior in the face of the Russia–Ukraine conflict. Energy Econ. 107413.
Zhang, F., Wen, N., 2022. Carbon price forecasting: a novel deep learning approach. Environ. Sci. Pollut. Res. 29 (36), 54782–54795.
Zhang, W., Wu, Z., Zeng, X., et al., 2023b. An ensemble dynamic self-learning model for multiscale carbon price forecasting. Energy 263, 125820.
Zhang, F., Xia, Y., 2022. Carbon price prediction models based on online news information analytics. Financ. Res. Lett. 46, 102809.
Zhang, K., Cao, H., Thé, J., et al., 2022. A hybrid model for multi-step coal price forecasting using decomposition technique and deep learning algorithms. Appl. Energy 306, 118011.
Zhang, K., Yang, X., Wang, T., et al., 2023a. Multi-step carbon price forecasting using a hybrid model based on multivariate decomposition strategy and deep learning algorithms. J. Clean. Prod. 136959.
Zhang, X., Li, Z., Zhao, Y., et al., 2023c. Carbon trading and COVID-19: a hybrid machine learning approach for international carbon price forecasting. Ann. Oper. Res. 1–29.
Zhao, Q., Wang, H., Lu, S., 2022. MLDQ feature embedding and regression modeling for distribution valued data. Inf. Sci. 609, 121–152.
Zheng, Z., Xiao, R., Shi, H., et al., 2015. Statistical regularities of carbon emission trading market: evidence from European Union allowances. Physica A: Stat. Mech. Appl. 426, 9–15.
Zhu, B., Wei, Y., 2013. Carbon price forecasting with a novel hybrid ARIMA and least squares support vector machines methodology. Omega 41 (3), 517–524.
Zhu, B.Z., Han, D., Wang, P., 2017. Forecasting carbon price using empirical mode decomposition and evolutionary least squares support vector regression. Appl. Energy 191, 521e530.
Zhu, B., Ye, S., Wang, P., et al., 2022. Forecasting carbon price using a multi-objective least squares support vector machine with mixture kernels. J. Forecast. 41 (1), 100–117.